Chapter 16
Nonstandard Light for Ultrafast Laser Microstructuring and Nanostructuring

Francois Courvoisier

Abstract Ultrashort laser pulses have revolutionized laser-matter interaction because they can deposit energy at extremely small scales. High-speed and controlled nanostructuring has become possible both at the surface of materials and inside transparent materials. Here, a specific class of beams is reviewed: the "Bessel beams" that are quasi-invariant along the propagation. They provide new avenues for controlling laser-matter interaction at extreme nanometric scales at the surface of materials but also within the bulk of transparent dielectrics. Of particular interest is the possibility to generate nanostructures with extremely high aspect ratio—length divided by diameter—, up to several 10,000:1 using single ultrafast laser pulses. The generation of nanoplasma using quasi-non-diffracting beams provides access to extreme material states and opens a drastically new regime for material nanostructuring. This chapter reviews the state of the art of the fundamental concepts of Bessel beams and their applications, particularly for high aspect ratio nanostructuring, drilling, and stealth dicing. More complex beam shapes, based on the same concept of conical flow of light, offer new perspectives for materials processing.

Keywords Bessel beams · Diffraction-free beams · Ultrafast laser beam shaping · High aspect ratio · Stealth dicing · Curved beams

1 Introduction

Chirped pulse amplification has enabled an evolution in laser structuring. High-energy, ultrafast laser pulses, i.e., with pulse duration typically between 50 fs to some tens of picoseconds, can generate a highly excited free electron gas in the cold lattice. This is possible not only in metals but also in dielectrics, thanks to

F. Courvoisier (✉)
FEMTO-ST Institute, Université de Bourgogne Franche-Comté, Besançon Cedex, France
e-mail: francois.courvoisier@femto-st.fr

the nonlinear ionization. At the surface of materials, the ultrafast character of the energy deposition produces a high contrast between the excited zone and the non-excited material. This opens the possibility to structure materials at the micrometer or nanometer scale. This chapter will particularly emphasize the structuring of transparent materials bulk at this extreme scale. One of the key aspects of the possibility to excite transparent materials via nonlinear ionization is that energy can be stored inside the bulk of the material with no modification on other surfaces. Femtosecond and picosecond lasers have therefore found a large number of applications during the last decade.

While early works were dedicated to inscribing in materials the tiniest modifications using highly focused Gaussian beams, it has been then recognized that beam shaping could bring new opportunities. Chapters 15 and 26 discuss the applications of beam shaping for laser micro structuring and nanostructuring. This chapter focuses on a specific class of beam shapes which is the "non-diffracting" or "diffraction-free" beams. The terminology has been brought by Durnin when introducing the zeroth-order Bessel beam which is a propagation-invariant solution to the wave equation [1]. The specificity of this beam is that it can maintain an extremely narrow focus, even below the wavelength, on extremely long distances, well beyond the limitation of the Rayleigh range. In solid dielectrics, the zeroth-order Bessel beam has close links with the filamentation of ultrafast pulses.

A first class of applications therefore lies in the use of this propagation invariance to circumvent the technical issue of maintaining the workpiece surface within the laser focus. A second very important property of Bessel beams is that their nonlinear propagation inside transparent materials can be also invariant, in contrast with the nonlinear propagation of Gaussian beams which is conventionally much more difficult to control. It will be seen that the second property allows for depositing energy highly homogeneously along extremely long distances. The generation of extremely high aspect ratio nanostructures can be performed even using a single-laser pulse. This has opened a large number of new applications. Among them, high-speed (meter per second) glass separation with a non-ablative process has attracted an enormous attention for obvious applications to mass fabrication of touchscreens, consumer electronics and, more recently, high-speed cutting of windshields and window glass. This field of research has rapidly evolved from the first reviews [2–6].

In this chapter, Sect. 2 describes non-diffracting Bessel beams, how they can be shaped, and the applications of their extended focal zone to laser surface microstructuring and nanostructuring. Section 3 discusses the propagation of intense ultrashort pulses inside the bulk of transparent dielectrics. The nonlinear propagation of Bessel beams corresponds to the asymptotic behavior of the filamentation process of a Gaussian pulse. It is shown that Bessel-shaped pulses can generate plasma rods with nanometric diameter over a length of several tens of micrometers to centimeters. The relaxation of a nanoplasma rod inside the transparent material can generate an index modification, nano-gratings, or a void. The physics of the interaction and of the void formation will be discussed. Section 4 reviews the applications to high aspect ratio microstructuring and nanostructuring of transparent dielectrics, with a particular

emphasis on stealth dicing. Section 5 is dedicated to the new perspectives in the field: additional beam engineering maintains the diffraction-free character without the cylindrical symmetry of the initial Bessel beam. Tailoring the beam structure can improve the stress field, with important applications to stealth dicing. Another important perspective is to engineer the ultrafast laser beam such that it can produce curved profiles inside the transparent material: this can be used to avoid mechanical chamfering that is conventionally used to avoid chipping of glass.

2   Propagation of Non-diffracting Beams in Vacuum: Application to Surface Laser Nanopatterning

This section first describes what are non-diffracting Bessel beams and the means to generate them. Then, the applications of their extended focus to surface nanostructuring are reviewed.

2.1   Non-diffracting Beams and Spatial Beam Shaping of Ultrashort Pulses

2.1.1   Basics of Bessel Beams

A Bessel beam can be seen as a cylindrically symmetric interference field: it is the coherent superposition of an infinite set of plane waves whose wavevectors are distributed on the generatrix of a cone. Durnin has formalized the Bessel beam as a solution to the Helmholtz equation: this solution is featured by an intensity distribution that is invariant along the propagation direction [1].

The monochromatic field scalar amplitude of the zeroth-order Bessel beam reads in cylindrical coordinates as:

$$A(r, z, t) = A_0 J_0 \left(\frac{2\pi}{\lambda} \sin \gamma r \right) e^{i \frac{2\pi}{\lambda} \cos \gamma z} \tag{16.1}$$

where λ is the wavelength, A_0 is constant, and γ is defined as the cone angle. This is the angle made by the wavevector with respect to the optical axis: the wavevector has a radial component $k_r^0 = \frac{2\pi}{\lambda} \sin \gamma$ and a longitudinal component $k_z^0 = \frac{2\pi}{\lambda} \cos \gamma$. It is apparent from the above equation that the intensity $|A|^2$ of the field is invariant with z.

Obviously, this solution carries infinite energy. In practice, the transverse profile is apodized, and the length of the Bessel beam is therefore limited. To simplify the terminology, no difference will be made between the ideal Bessel beams and
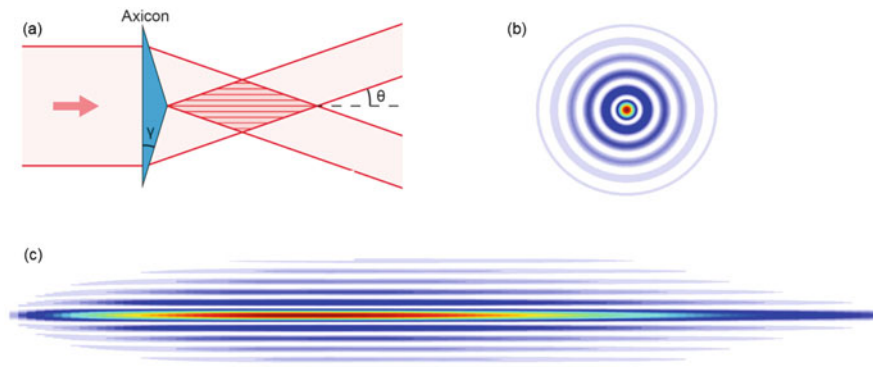
Fig. 16.1 (**a**) A Bessel beam is a cylindrically symmetric field of interference and can be, for instance, generated using an axicon lens. (**b**) Example of a transverse cross section of the intensity distribution. (**c**) Longitudinal cross section of the intensity distribution. The intensity scales from blue (low) to red (high)

the experimentally realized ones. In addition, unless explicitly specified, the zeroth-order Bessel beam will be called "Bessel beam."

Figure 16.1 shows how the interference field defines the length over which the Bessel beam exists. It is also apparent that the number of lobes around the central core is, during the propagation, progressively increasing and then decreasing. The Bessel zone length is typically defined by $Z_{\text{max}} \sim w/\tan\gamma$, where w is typically the waist of the input Gaussian beam.

Within the Bessel range, since the angle made by the interfering waves does not change along propagation, the central lobe diameter is invariant. The full width at half maximum of the central lobe intensity profile is $0.36\lambda/\sin\gamma$, and the first zero of the intensity is given by $r_0 = 0.38\lambda/\sin\gamma$. In the Fourier space, i.e., the far field, the Bessel beam intensity distribution is a ring, peaked at $k_r = k_r^0$, with a thickness inversely proportional to the length of the Bessel zone.

A Bessel-Gauss beam is one of the experimentally realizable Bessel beams. It can be generated by shaping a Gaussian beam using an axicon. The on-axis intensity distribution of a Bessel-Gauss beam propagating in a medium of index n with a cone angle γ in the medium can be expressed using the input power P_0 and waist w_0 of the Gaussian beam using the following expression, within the paraxial approximation [7, 8]:

$$I_{\text{on-axis}}(z) = 8\pi P_0 nz \frac{\sin^2\gamma}{\lambda w_0^2} e^{-2(z\sin\gamma/w_0)^2} \tag{16.2}$$

In the close vicinity of the central lobe, one can therefore approximate the Bessel-Gauss beam intensity profile to $I(r, z) = I_{\text{on-axis}}(z)|J_0(k_r^0 r)|^2$.

While for a Gaussian beam the Rayleigh range shortens when the beam is more focused, i.e., when the waist is smaller, the situation is very different for a Bessel

beam since the cone angle γ and the waist w are two independent parameters. Therefore, the central core width can be down to nearly $\lambda/2$, while the Bessel zone length can be arbitrarily chosen—obviously within the limits of the numerical aperture of the optics.

The Bessel beam can also be seen as an elongated focus, as it was initially shown by McLeod [9]. The energy flow is conical, and, within a geometric optics point of view, the energy is focused onto a segment instead of a point for the Gaussian beam. Increasing the length of the Bessel beam by a factor 10 only requires to increase the waist in a similar factor, and if one wants to maintain the peak intensity, the input power must be adequately increased.

2.1.2 Spatiotemporal Structure

The spatiotemporal structure of the Bessel beam created using an ultrafast pulse is a coherent superposition of monochromatic Bessel beam amplitudes. The relationship between the different components is determined by the way the pulse is shaped. For instance, axicons or spatial light modulators do not create the same spatiotemporal structure [10]. However, to the best of our knowledge, the exact spatiotemporal structure of the Bessel beam has no impact on laser nanostructuring. This is why, in the following, the pulses will be treated using monochromatic approximation.

2.1.3 Presence of Interfaces

Importantly, when the beam crosses a flat interface at normal incidence such as air dielectric or dielectric air, the transverse profile does not change. This is because the radial wavevector is preserved [11]. The Bessel zone length is increased by a factor n, the refractive index of the medium. It is also important to highlight the fact that the far field of the Bessel beam is composed only of a thin radial spectrum implies that the Bessel beam is much less sensitive to spherical aberration when the beam is focused inside a dielectric medium. This is an important benefit in comparison with Gaussian beams which are distorted in this situation.

2.1.4 Bessel Beam Generation

Bessel beams can be generated using several means. All are intended to apply a conical phase onto the Gaussian laser beam: spatial light modulators (SLM) [12, 13], diffractive optical elements [14, 15], transmissive [16–19], or reflective axicons [20]. However, it is conventionally difficult to obtain high cone angle after such shaping means. Spatial light modulators and diffractive optical elements are limited to cone angles below some mrad. The fabrication of axicons is also technically very difficult, particularly when the cone angle is above some degrees. The mechanical turning often induces defects in the symmetry around the optical axis [21]. In addition,
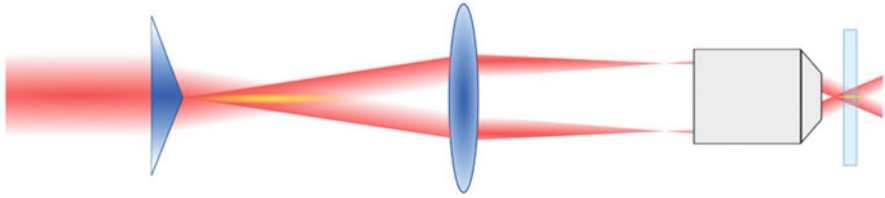
Fig. 16.2 Setup used to increase the cone angle of a primary Bessel beam. The lens and microscope objective are placed in a 2f-2f configuration to image the primary Bessel beam. Copyright Remi Meyer
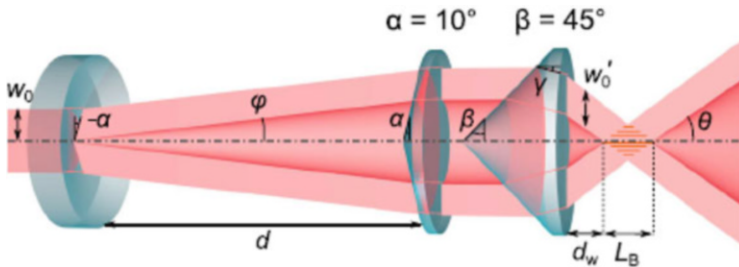

Fig. 16.3 Setup to generate extended Bessel beams with high cone angles and a long working distance (indicated as d_w). Reprinted figure with permission from [27]

the tip of the axicon is very often rounded, which generates a spherical wave co-propagating and interfering with the Bessel beam [22, 23]. Recently developed laser-based techniques avoid the defect of cylindrical asymmetry due to the mechanical interaction between the tool and the workpiece [24, 25].

As it will be seen in Sect. 3.4, the applications to nanostructuring often require strong focusing typically above 10 to 20°. Most of the high-angle Bessel beam generators are similar to the one shown in Fig. 16.2. They are based on imaging a first Bessel beam using a 2f-2f telescopic arrangement which magnifies the cone angle at the cost of reducing the beam length by the square of the magnification. With this kind of architecture, the Bessel zone length is typically below a few hundreds of micrometers for a cone angle exceeding 10°.

Recently, a new kind of architecture has been developed to reach Bessel zone lengths of several millimeters. A first version has been developed by Chebbi et al. [26]. This has been recently improved in [27] to avoid any intermediate focusing. As shown in Fig. 16.3, the first two axicons are complementary and create a wide annulus of light that is further focused using a very high-angle axicon.

The intensity over the optical axis of Bessel-Gauss beams varies smoothly. By controlling the diffraction efficiency of the phase mask applied by spatial light modulators or diffractive optical elements, it is possible to generate Bessel beams where the on-axis intensity is nearly constant over a segment, which is important for applications to laser nanostructuring [28, 29]. A new approach using geometrical phase optics has been developed for the same purpose in reference [30].

2.2 Extended Focal Length and Applications to Surface Structuring

Ultrafast laser ablation is characterized by a very marked threshold. Nanostructuring is made possible by adjusting the sample area over which the fluence exceeds the ablation threshold. Nanostructures can be processed with diameters even well below the wavelength [31]. For this application, the laser distribution must have strong gradients. This is conventionally performed using tightly focused Gaussian beams, as shown in Fig. 16.4a. However, in this case, the longitudinal positioning range over which the surface of the solid can be nanostructured is on the same order of magnitude as the diameter of the structures. This renders the sample positioning critical which is generally an obstacle to large area processing for real-life applications.

In this context, the quasi-arbitrary length of the Bessel zone allows fully lifting this constraint. A number of works have demonstrated surface nanostructuring using Bessel-Gauss beams, including processing of non-flat samples or opto-perforation of cells, in which position is inherently difficult to control [18]. The submicron ablation of indium tin oxide (ITO) has been demonstrated by Sahin [32], and Doan et al. demonstrated the ablation of transparent conductive oxide through the substrate, so as to improve the final surface quality [33]. The extended Bessel zone allows for compensating flatness and thickness variation of the sample. The same property holds for higher order Bessel beams, used by Wetzel to process graphene [34], and holds more generally for all extended interference fields [35, 36]. Recently, the process has been extended to homogeneously write nano-ripples at the surface on a highly curved sample [37], as shown in Fig. 16.4b.

The longitudinal invariance of a Bessel beam is also useful to produce high aspect ratio microstructures inside metallic or dielectric materials by percussion drilling. Indeed, even when it is partially obstructed, the Bessel beam maintains its structure, obviously over a shorter length. Alexeev et al. demonstrated that a Bessel beam maintains a higher intensity over a longer length than Gaussian beams when propagating inside a deep channel made inside a metallic sample [38]. It is also noticeable that tapering occurs very frequently on most high aspect ratio structures in opaque materials [39]. In diamond, graphitization occurs very rapidly after few laser pulses, such that tapering also occurs when drilling trenches [40, 41].

Another important property of Bessel beams is that they are self-healing: after an obstacle, the intensity maximum reconstructs because of the conical flow of light. Nguyen et al. have used this property, in addition to the extended Bessel zone, to create high aspect ratio microstructures in additive manufacturing. The presence of the powder only moderately effects the beam structure [42].
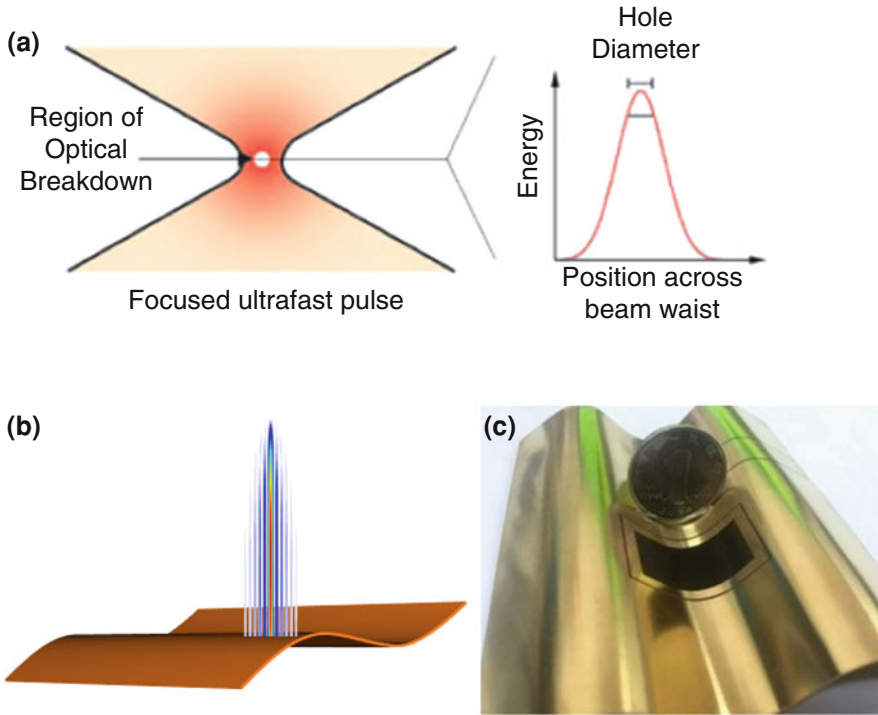
Fig. 16.4 (**a**) Optical breakdown can be induced on lateral dimension much smaller than the spot size, but it also implies that the longitudinal extent over which the sample surface is placed is restricted to the same order of magnitude [31]. (**b,c**) The central lobe of diffraction-free Bessel beam provides a large longitudinal range where identical illumination conditions can be obtained. Li et al. demonstrated homogeneous laser nanoprocessing on non-flat sample [37]. (**a**) Reprinted figure with permission from [31]. Copyright (2004) National Academy of Sciences, USA. (**c**) Reprinted figure with permission from [37]. Copyright The Optical Society

3 Non-diffracting Beams for High Aspect Ratio Nano-structuring the Bulk of Transparent Materials

The most striking benefits with Bessel beams in terms of laser materials processing lie in the processing of transparent materials, particularly in a near-single burst illumination regime. This section discusses the propagation of relatively high-intensity pulses, from regimes where they are used for two-photon photopolymerization to regimes where the laser-deposited energy density is high enough to open a void inside the transparent solid. The related applications will be discussed in the next section.

3.1 Propagation in the Bulk of Transparent Dielectrics and Nanoplasma Formation

When propagating inside a transparent dielectric, ultrashort pulses undergo the nonlinear self-focusing Kerr effect, and if the intensity is sufficiently high, an electron-hole plasma is generated. This plasma both partially absorbs and defocuses the pulse. These multiple effects are obviously highly nonlinear: the filamentation regime where all these effects are combined is very difficult to predict and to scale. Gaussian beams in the filamentation regime undergo a strong spatial and spectral reshaping [43]. The physics of the nonlinear propagation of Bessel beams differs significantly from the one of Gaussian beams. It has been described in detail by Polesana et al. [44].

In a pure Kerr medium, in the absence of losses, an ultrafast Bessel beam undergoes reshaping by four-wave mixing. Several new spatio-spectral components are generated: a wave parallel to the optical axis and a wave with the radial wavevector $\sqrt{2}k_r^0$ [45]. Engineering the spatial spectrum of the Bessel pulse can stabilize the beam [46, 47], but, with the perspective of laser structuring, most of the stabilization can come from nonlinear losses occurring within the central core. Porras et al. demonstrated the existence of stationary solutions, i.e., propagation-invariant, based on a conical flow of light associated with nonlinear losses, even in the presence of Kerr effect. These solutions can be seeded using Bessel beams. Noticeably, the stationary regime exists when both cone angle and nonlinear losses are sufficiently high. The non-stationary regime of the filamentation of Bessel beams can be associated with the periodic formation of plasma with applications to the imprinting of periodic marks inside fused silica [45].

When the cone angle is sufficiently high, the impact of Kerr effect becomes negligible. The length over which an optical ray crosses a high-intensity region is limited to about 1 μm, which implies that the accumulated Kerr phase is close to zero. In addition, when the cone angle is high enough, stabilization occurs from the high nonlinear losses due to nonlinear ionization and plasma absorption [44]. In this case, a plasma rod can be generated within the central core of the Bessel beam. The plasma density is highly homogeneous, and the applications reviewed below take benefit of this homogeneity.

Garzillo and co-workers experimentally compared the propagation of femtosecond and picosecond pulses in BK7 glass [48]: the picosecond regime seemed to be more stable than the femtosecond one. In practice, picosecond pulses undergo less spectral reshaping and less plasma defocusing. Another argument was raised by the group of R. Stoian (Univ. Lyon-Saint Etienne, France): using numerical simulations shown in Fig. 16.5, the group pointed out that the higher peak power of femtosecond pulses tend to enable ionization over a wider transverse distance than the picosecond ones. The picosecond regime therefore seems more favorable to a higher localization of energy deposition within the Bessel beam central lobe. It should be however noted that the vertical scales of the graphs are not identical: the higher dynamical range for the case of 1.8 ps pulses makes it in fact difficult to quantitatively compare. More investigations are therefore needed.
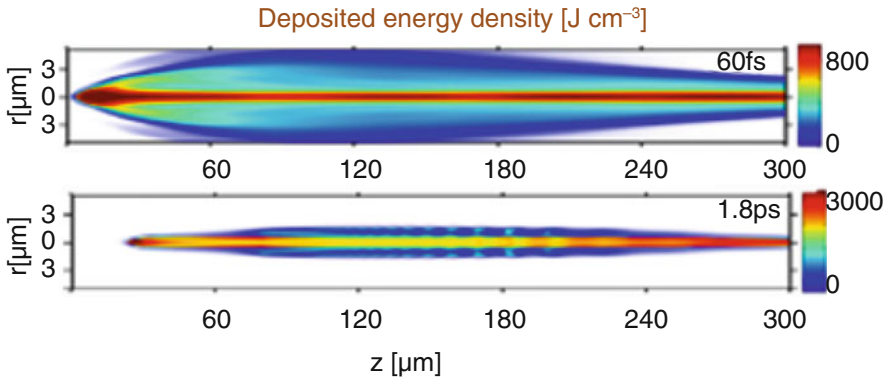
Deposited energy density [J cm⁻³]

Fig. 16.5 Comparison of energy deposition by a Bessel beam within fused silica using nonlinear Schrödinger equation for a single pulse of duration 60 fs pulse (top) and 1.8 ps (bottom). Reprinted figure with permission from [49]. Note that the color bars are different. The energy density in the picosecond case seems less homogeneous

It is worth noticing that these results are formulated on simulations based on paraxial nonlinear Schrödinger equation. It is an approximation to Maxwell's equations obtained after neglecting longitudinal components of the field, and the plasma is treated as a static medium of permittivity fixed by Drude model [50]. This approach eliminates the possibility of modeling plasma waves. Although these approximations are extremely useful to model the filamentation dynamics inside solids [43, 51], they are in fact no longer valid under strong focusing conditions to model the interaction with nanoscaled plasmas. This is even more true when the plasma density reaches the critical density, at which the permittivity turns to zero. Beuton et al. predicted with a full Maxwell code the possibility of reaching overcritical plasma densities [52]. The additional effect of resonance absorption has been very recently demonstrated to occur in these conditions for a femtosecond Bessel beam: most of the absorption is collisionless [53]. This is an effect which was not captured by the models described above, and that will be discussed at the end of this section.

3.2 Link to the Filamentation of Gaussian Beams

The propagation of Bessel beams inside solid dielectrics has been popularized because it is a close cousin of the filamentation of Gaussian beams. More precisely, during the nonlinear filamentation process, Gaussian beams self-reshape into Bessel-like beams [54]. Filaments and Bessel beams in the presence of nonlinear losses are both characterized by an intense central core, surrounded by an energy reservoir. Nonlinear stationary Bessel beams can be seen as the asymptotic structure
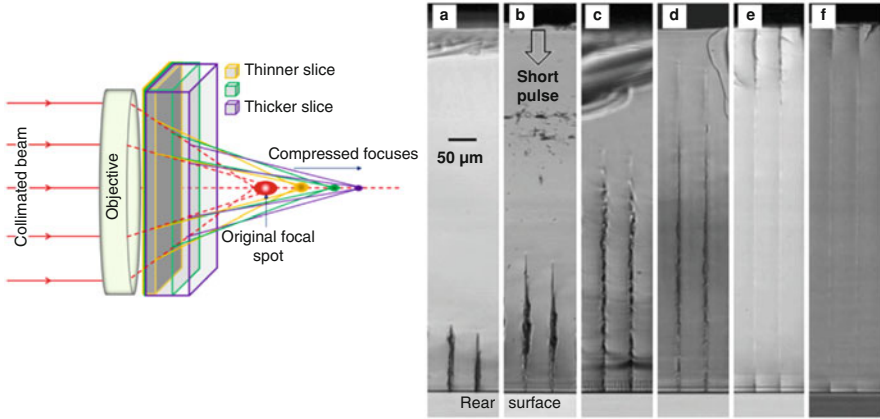
Fig. 16.6 (Left) Concept of the spherical aberration induced by a thick glass slide inserted after the focusing objective (right) views of cleaved surfaces of the longest single-shot voids fabricated with different inserted glass plate thickness: (**a**) no glass, (**b**) 1 mm, (**c**) 2 mm, (**d**) 3 mm, (**e**) 5 mm, (**f**) 6 mm. Reprinted figure with permission from [58]

of filamentation after a long propagation distance where the dynamics becomes stationary, i.e., propagation-invariant.

To efficiently trigger filamentation, most authors use high-power pulses or bursts of pulses with either moderate focusing to induce a dynamic reshaping by Kerr effect or, more often for laser structuring applications, a relatively high focusing associated with spherical aberration [55–57]. Spherical aberration focuses the field components with the strongest radial wavevectors first, while the weakest radial wavevector components are focused at longer propagation distances. This way, a Gaussian beam with spherical aberration closely resembles to a Bessel beam (see Fig. 16.6(left)). Ahmed et al. exploited this property by inserting a thick plate of fused silica between the focusing lens and the transparent workpiece where the filamentation had to be created [58] (Fig. 16.6(right)). This enables a high degree of control of the filamentation, very close to what be achieved using geometrical optics to control the position of the Bessel beam. Recently, Alimohammadian et al. used conical phases in the Fourier space to strengthen the filamentation and to longitudinally shift the position of the filament inside transparent materials by several hundreds of micrometers [59, 60].

3.3 High Aspect Ratio Index Modification

Using a Bessel beam with moderately high fluence (typ. 10^{13} W.cm^{-2}), a subcritical plasma is generated inside transparent dielectrics. This has been characterized, for instance, by Velpula et al. using a two-color time-resolved microscopy [61]. The
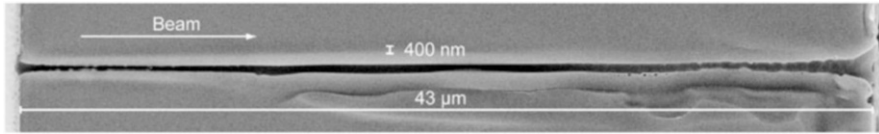
Fig. 16.7 High aspect ratio nanochannel generated by a single pulse of a Bessel beam with cone angle 11° in glass. Reprinted figure with permission from [8]

plasma of excited free electrons relax as heat or via self-trapping which induce structural rearrangements as described in [62] to yield positive or negative index modifications depending on the material and the relaxation pathway. This regime was used in early works to generate a homogeneous index modification inside glass [63, 64] by using low cone angles.

3.4 High Aspect Ratio Nanovoid Formation

3.4.1 Single-Shot Drilling

Interestingly, if the input pulse energy and the focusing of the Bessel beam are strong enough, a single-laser pulse is enough to generate a high aspect ratio nanovoid inside glass, which was first demonstrated in our group [8]; it is shown in Fig. 16.7. With Gaussian beams, void opening was also observed previously, but much stronger focusing is required, typically with numerical apertures close or above one [65, 66].

The filamentation regime where a Gaussian beam nonlinearly self-transforms to generate a relatively homogeneous nanoplasma can also deposit sufficient energy density to open elongated nanovoids, for instance, in PMMA [56] or glass [59, 60, 67].

One can remark here that this regime is significantly different from what can be generated using temporal Airy pulses, where it is the plasma dynamics that induces a spatial reshaping. This generates an elongated filament, typically on the order of 30 μm , and a high aspect ratio channel close to the surface of glass [68, 69]. This regime is reviewed in detail in Chap. 17.

The observation of these high aspect ratio voids with nanoscale diameter, under scanning electron microscopy (SEM), is particularly challenging. Several techniques have been developed throughout the years: initially, Bhuyan et al. were mechanically cleaving the channels. To increase the reliability of the imaging, focused ion beam (FIB) milling was used later [70]: using the ion beam, a large cuvette is first drilled in the vicinity of the void, providing access to the SEM beam to image the vertical plane containing the longitudinal cross section of the void. Then, a very fine approach, removing progressively the material by vertical layers of typically 40 nm and intermediate imaging, allows imaging the nanoscale void with high resolution. Importantly, this process is overall very long ($\approx$ 1h per void),

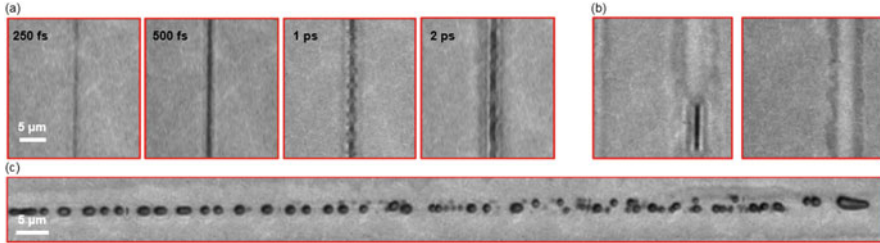**Fig. 16.8** (**a**) Different morphologies of material modification after single-shot Bessel beam illumination with the same pulse energy with different pulse durations. (**b**) Modification inside Gorilla glass, for a 3 ps pulse, at two different positions inside the sample. (**c**) Same as in (**b**) with three times higher pulse energy. Reprinted figure with permission from [73]

limited to depths of approximately 30 μm, and the void channel must be perfectly perpendicular to the sample surface such that the FIB beam milling is parallel to the high aspect ratio void. Very recently, Chen et al. developed an efficient technique to overcome those difficulties: the drilling of void channel is repeated at different longitudinal positions inside the sample, and then fine polishing of the sample surface provides access to the transverse cross section of the voids at different heights using SEM. A 3D reconstruction is then possible [71].

High aspect ratio void formation has been observed in a very large number of transparent materials, such as fused silica, different glasses, chalcogenide glasses, and PMMA, ZnS [72] , and even in materials as hard as sapphire [70]. The void opening requires a strong gradient of energy deposition, associated with relatively fast cooling. Importantly, the modification produced inside the transparent material is not always a void particularly at the highest energies. In this case, it is very often that irregular bubbles form in the position of the Bessel beam central core. This typically occurs when a relatively large diameter of material has been melt around the void. Depending on the material, the highest energies can be associated with the formation of an index modification on a large diameter. Figure 16.8 shows several types of modifications created in different materials with various parameters.

3.4.2 Influence of Pulse Duration

Figure 16.9 compares the modification created in sapphire for two different pulse durations under relatively strong focusing ($\gamma = 26°$ in air). In the femtosecond case (top left), the void channel is free from apparent defects under SEM imaging, while the picosecond case (top right) shows a much wider heat-affected zone and redeposited nanoparticles. In the latter case, it is apparent that the void opening was associated with a transient hot vapor phase where nanoparticles could nucleate. It is still unclear which of the picosecond or the femtosecond case is associated with the highest energy density. Void formation in the femtosecond case is still under debate as it will be seen below.
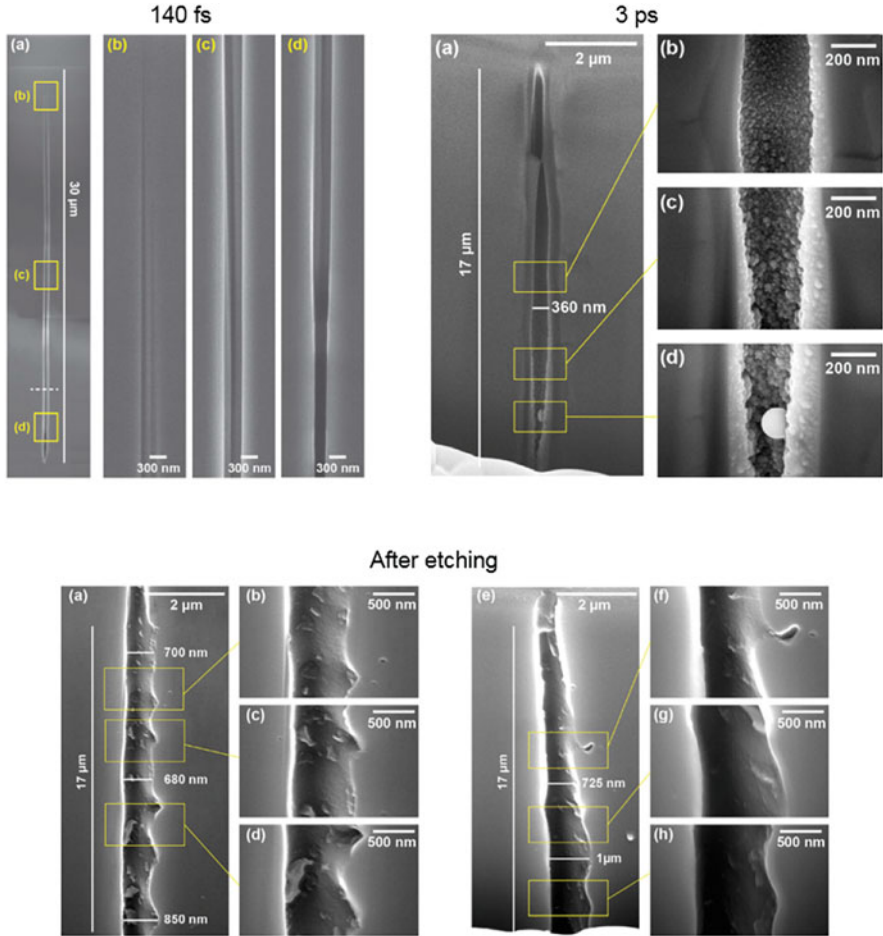
Fig. 16.9 High aspect ratio nanovoids generated in the bulk of sapphire in the single-pulse regime using a Bessel beam with cone angle 14°. (Left column) pulse duration of 140 fs; (right column) pulse duration of 3 ps; (top row) SEM imaging after FIB milling; (bottom row) after HF etching of the FIB-milled structures. The picosecond case shows a larger heat-affected zone and cracks. Adapted figure with permission from [70]

It is important to remark that high aspect ratio nanovoids can be created using both femtosecond and picosecond pulse durations, but, in the femtosecond regime, stronger focusing is needed (cone angle typically above 10° inside the solid). In this high focusing condition, voids could be opened using pulse durations down to 50 fs, where, conventionally, avalanche ionization cannot be triggered. This shows that the physics of the interaction, at least in the femtosecond regime, is not yet fully understood. In glass and fused silica, picosecond pulses generally yield modifications that are more visible under conventional microscopy: they are

probably wider and show a wider heat-affected zone. Some modifications extend several micrometers away from the channel center (see, for instance, Fig. 16.2 of reference [74]).

3.4.3   Bursts

It can be interesting to investigate the reduction of peak power by splitting the pulse into several sub-pulses so as to reduce nonlinear ionization in the outer lobes of the Bessel beam.

In the void formation regime in glass, our group has investigated the effect of splitting the femtosecond pulse in two equal sub-pulses, separated by durations between 0 and 500 ps [75]. Below a pulse separation of approximately 10 ps, the morphology and length of the void were varying shot to shot. But interestingly, above a pulse separation of 10 ps, the voids that were formed could have increased diameter in comparison with a single-shot case, and smaller energies could give rise to smaller diameter voids. In this case, a diameter close to 100 nm could be reached.

Using absorption measurements, it was shown that the overall absorption was not increasing in comparison with the single-pulse case. Therefore, the increase of drilling efficiency is due to an increased energy density deposited by the sequence of two pulses. The material after the first shot undergoes a progressive transformation on a scale of typically 10 ps: in this hot dense state, the material is highly absorbing. This result matches the pump-probe measurements of Garcia-Lechuga at the surface of fused silica [76] as well as simulation results predicting the transformation of fused silica into warm dense matter when the laser-deposited energy density reaches several MJ/kg [77, 78] as it is the case after the first pulse the Bessel beam configuration [75]. This state is long-living, probably more than several nanoseconds [79], which is why the enhancement of drilling efficiency is observed for bursts of pulses separated by up to several tens of ns as characterized by Kumkar et al. [80, 81] and frequently used in the application of stealth dicing, which is described in the next section.

Depending on the exact geometrical configuration, some transient wave-guiding effect has been observed, to increase the length of the modification. This is possible for relatively low cone angles, where the beam can be trapped into the waveguide created by the first pulse [82]. More generally, burst pulse configuration can benefit of the heat accumulation to create wider and stronger modifications. Although the burst configuration has been successfully used for stealth dicing, systematic comparisons of the diameter evolution with the burst parameters have still to be performed.

3.4.4   Pulse Polarization

In fused silica and glass, no effect of the pulse polarization has been yet observed. Although it can slightly modify the ablation threshold because of the difference in

nonlinear ionization cross sections, the cross sections of the channels are circular
whatever the polarization. In contrast, in sapphire, voids generated using a linear
polarization, in the femtosecond regime, have an elliptical transverse cross section,
oriented perpendicularly to the polarization direction [53]. The ellipticity can be
used to control the formation of cracks [70]. In the picosecond regime, for pulse
durations above 600 fs, high-power Bessel beams create cracks in several directions,
which indicates that the void cross section is circular [83].

3.4.5 Heat-Affected Zone

The formation of high aspect ratio voids fully enclosed in sapphire or glass
demonstrates that part of the material is compressed around the void. In the case
of sapphire, Rapp et al. evaluated the compression ratio to ∼15% [70].

Recently, using FIB milling and chemical etching, Zhang et al. characterized that
around the 290 nm-diameter void channel drilled in fused silica with 4 ps pulses, the
material is annealed over a diameter of ∼ 2 μm, corresponding to the Bessel beam
core, and cracks develop only at a further distance, typically 2 μm (see Fig. 16.10)
[84]. These micro-cracks are key for the application to stealth dicing mentioned in
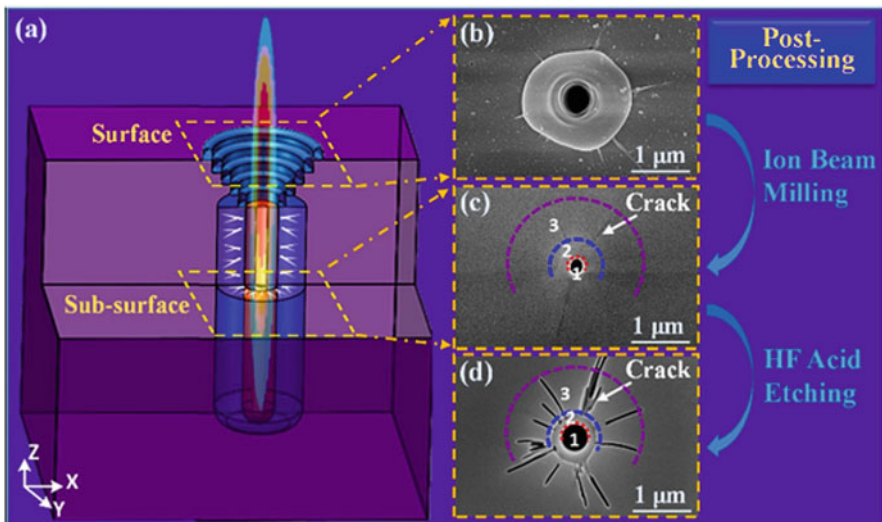Sect. 4.

Fig. 16.10 SEM imaging of a void transverse cross section inside fused silica. In (**c**), the void is
inside the red dotted line (1), the annealed region (2) is enclosed in the blue circle, and the third
region with cracks is within the purple circle. (**d**) Shows the same area after HF etching to reveal
the cracks. Reprinted figure with permission from [84]

3.5 Physics of Energy Deposition and Void Opening: Current Challenges

The physics of the energy deposition process is particularly difficult to characterize because of the nanometric value of the characteristic scales involved. A very interesting discussion on experimental flaws is provided in Section II.B of reference [85]. This field has been very active in the recent years, with several techniques that were developed to characterize the nonlinear pulse propagation and energy deposition inside transparent dielectrics. Bergner et al. developed a pump-probe microscopy technique to image the filamentation of 6 ps pulses [86]. Their technique was capable to retrieve the local index of refraction. This technique was particularly efficient to show the impact of Kerr effect ahead of the focal region, the buildup of the plasma which particularly extends in time toward the laser source. One can notice also that their results demonstrate that the region where the maximal temperature is reached, around the Gaussian beam focus, is maintained hot during several nanoseconds at least, in agreement with the results mentioned in Sect. 3.4. This is the region where the strongest material modification is observed. The spatial resolution of this technique is unfortunately not enough to characterize the formation of nanovoids.

As it was mentioned earlier in Sect. 3.1, the energy deposition during the pulse propagation has not yet been completely modeled. The computationally efficient models using nonlinear Schrödinger equation cannot describe the detail of the physics occurring when submicron plasma is generated. Using first-principle particle-in-cell numerical simulations that are based on solving Maxwell's equations together with particles trajectories [87, 88], our group has recently demonstrated that a very important absorption mechanism was collisionless, which is conventionally very difficult to capture using simulations [53]. This collisionless absorption is a combination of two effects. The first is resonance absorption: when a p-polarized pulse impinges on a plasma ramp, the pulse is deviated at the so-called turning point where the density reaches $\rho = \rho_c \cos i$, where ρ_c is the critical density and i the incidence angle on the plasma. (Note that for Bessel beams, the turning point shifts away from the optical axis when the cone angle $\gamma = \pi/2 - i$ is decreased). The evanescent field created from the turning point tunnels to the critical density point where it can resonantly excite electrostatic plasma waves—also named Langmuir or longitudinal waves in the literature [88]. If the turning point and critical point are close enough, the conversion efficiency can be very important, typically up to 60% [89]. The second effect is the damping of the plasma wave by several plasma wave-particle interaction processes such as Landau damping and transit acceleration. These interactions are collisionless processes [88]. Overall, in conditions close to the regime of nanovoid formation with femtosecond pulses (e.g., [8] and [70]), our simulations demonstrated that over 90% of the absorption is collisionless. This shows that most of the literature models still have to be adapted to fully interpret the dynamics of plasma buildup and laser-plasma interaction during the pulse propagation.

After the energy has been deposited in the form of an electron-hole plasma inside the dielectric, a number of relaxation processes take place. They highly depend on the energy density that was deposited by the laser pulse. For relatively low ionization degree, the free electron relaxation involves phonon excitation, generation of self-trapped excitons, themselves relaxing in the form of structural deformations. However, for the case of void opening, it is more likely that high energy densities are involved. When the ionization percentage typically reaches 20% (see the case of silicon in reference [90]), lattice disordering can occur at ultrafast scales [91], yielding bandgap shrinking, as observed recently in fused silica by Winkler et al. [92].

A number of experiments corroborate the fact that a fast transition to a hot state arise approximately in the picosecond scale after the laser pulse. Somayaji et al. reported the absence of trapping at the sub-picosecond scale in fused silica [79], while the trapping of free carriers occurs within 150 fs in the case of weak ionization [93]. The same authors also reported photoluminescence and spectrally resolved photoluminescence at the ns scale, demonstrating a phase on the order of 5000 K, well above the boiling point of silica and close to its critical point [94]. This is consistent with the observation of a transformation at ps-scale toward a regime of warm dense matter by Hoyo et al. [75] as well with the refractive index measurements on the filamentation of picosecond Gaussian beams of reference [86]. Heat diffusion occurs during several hundreds of nanoseconds, in association with potential phase changes.

Two scenarii were discussed for the actual opening of the void structure. References [95] and [65], considering the voids formed by tightly focused Gaussian beams, first hypothesized a mechanism where the pressure reached by the plasma creates a microexplosion that compresses the solid material around. Numerical simulations based on elastoplastic modeling including the equation of state of fused silica showed the feasibility of this mechanism for an ultrafast Bessel pulse. In this mechanism, the void would open on timescales of several hundreds of picoseconds [52, 96].

Bhuyan et al. used phase contrast microscopy to characterize the dynamics of plasma and void formation using femtosecond and picosecond pulses, shaped as Bessel beams [97, 98]. The measurements shown in Fig. 16.11 seem to show that the void opening takes place between 1 to several milliseconds after the laser pulse. A second mechanism has therefore been suggested: cavitation could occur within an overheated liquid [98]. Similar dynamics is observed using picosecond pulses [79]. However, the experimental setup cannot distinguish the radial distribution of the index of refraction. It is possible that the high temperature reached around the microexplosion site, with a high positive refractive index contribution, could mask part of the process at early times. For now, the differences observed between the femtosecond and picosecond regime in terms of void morphology (Fig. 16.9) are not yet fully explained. More experimental and simulation works are required to fully answer this question. Finally, one can remark that, in the case that warm dense matter is actually generated in the relaxation of the plasma, this state of matter is still challenging to model and is not described by the Drude model [99].
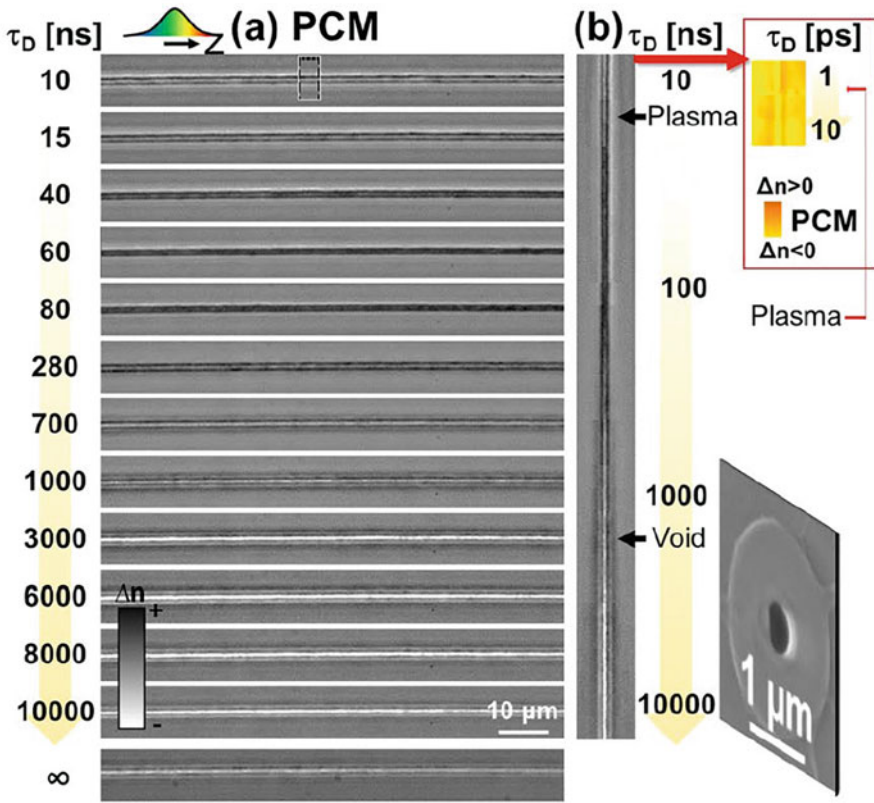
Fig. 16.11 (**a**) Time-resolved sequence of phase contrast imaging corresponding to the appearance of a high aspect ratio void inside fused silica after illumination by a chirped pulse of 5 ps duration (propagation from left to right). (**b**) Concatenation of crosscuts of the images of (**a**) to show the evolution of the dynamics in time (log scale). The inset shows the dynamics at early times in identical conditions, from [98]. Reprinted figure with permission from [79]

4 Applications to High Aspect Ratio Nanostructuring

Ultrafast non-diffracting Bessel beams have been successfully used in a number of applications where high aspect ratio microstructure or nanostructures are required.

4.1 Two-Photon Photopolymerization

Two-photon photopolymerization is a powerful fabrication technique to produce almost arbitrary-shaped components and tools, scaling from millimeters to sub-micrometer, useful to a wide range of applications [100–102]. However, point-

by-point irradiation is a very slow process. Zeroth and higher-order Bessel beams have been used to parallelize the process and produce two- or three-dimensional structures by avoiding the translation of the beam in one or more directions (see [2] and references therein, [103, 104]).

4.2   Index Modifications and Gratings

At low fluence, the long, subcritical plasma channels created by ultrafast pulses shaped as Bessel beams in the single-shot or multishot regime induce a local modification of the index of refraction. These modifications are highly homogeneous and can be positive or negative depending on the material [105]. Glass photosensitivity can also be used to control the laser-induced modifications [106]. High aspect ratio smooth modifications were successfully used to generate volumetric Bragg gratings in PMMA, PDMS, or fused silica by a number of different groups [107–110]. Because of the width of the heat-affected zone, the modifications cannot be processed arbitrary close to each other, and the laser inscription often imposes operating on higher order of the Bragg grating. Still, the reflectivity of these gratings could reach up to 90% [110]. Reference [111] demonstrates extremely efficient passband and stop bands nearly with transmission of, respectively, nearly 100% and 0%.

The stress field induced within the material by the laser-induced modifications can interestingly be shaped to generate engineered optical anisotropies. In this context, Bessel beam provides a means to create optically thick modifications [112].

High aspect ratio modifications in fused silica and glass can be etched using hydrofluoric acid (HF) or potassium hydroxide (KOH), so as to serve for micro-fabrication purposes. Several works have been performed to increase the etching efficiency, particularly using double-pulse illumination to benefit from the localized absorption of self-trapped excitons [113, 114].

Finally, one can remark that in a near ablation regime, using a high number of pulses, self-organized nanovoids appear. They are shaped as lamellas oriented perpendicular to the polarization. Bessel beams allow for generating such gratings over extended volumes, as shown and modeled by Rudenko et al. [115, 116]. They find applications in laser fabrication of photonic components with space-varying anisotropy.

4.3   Laser Welding

Joining materials is required in almost all fabrication fields and scales. Because it is highly flexible and contact-free, laser welding is obviously highly attractive. Ultrashort laser pulses allow for welding glass and more generally transparent materials between themselves as well as glass with another material. The ultrashort

character of the pulses provides, via nonlinear ionization, the ability to control in three dimensions the position of the heat source. However, welding requires generally a relatively large volume of molten material to fill the small gap between the parts to be joined. Filamentation and Bessel beams are ideally positioned to locally fuse the transparent material over an elongated volume and relax, in addition, the constraint on surface positioning. The idea has been very early developed by Tamaki et al. and further developed by several groups [117–119]. The use of actual Bessel beams is more recent [120]. Importantly, the joined parts can become as strong as the bulk material itself. The illumination strategy, including heat accumulation using long burst, is an important factor to release the constraints and improve the stiffness of the weld parts [119]. Hecker et al. highlighted the role of the conical structure of the Bessel beam to maintain a homogeneous illumination during melting [121].

4.4 Nanovoids for Photonics

To build in-line spectrometers, it is necessary to have the means to extract a fraction of the light traveling inside optical waveguides. High aspect ratio nanovoids can be used as very efficient scattering centers for this purpose. The high index contrast provided by the void highly increases the efficiency for the light extraction in comparison with a more conventional index modification on the order of 10^{-2}. This has been nicely demonstrated to build spectrometers for astro-photonics, operating in the mid-infrared window, with waveguides and light extraction written inside a chalcogenide glass [122, 123] as illustrated in Fig. 16.12. Using a similar approach, reference [124] demonstrates very strong Bragg resonances for Bragg filters in the telecommunications window. The group of P. Herman, Toronto, corrected the aberration due to the curvature of optical fibers to laser-inscribe a chirped array of high aspect ratio nanovoids on a relatively short extent of the waveguide, not only to extract light out of the waveguide but also to focus the output-coupled light directly onto a camera without a lens. In this case, the nanovoids were also enlarged using chemical etching [125].

A second application of nanovoids is the fabrication of photonic crystals. However, as already mentioned, it is difficult to process voids very close to each other because of the diameter of the heat-affected zone and because the previously drilled channels impact on the Bessel beam propagation. However, for this application, it is not necessary that the aspect ratio is extremely high. Liu et al. have engineered the Bessel beam length to reduce the aspect ratio and produce relatively compact photonic crystals [126, 127]. In addition, at the air-solid interface, the voids often show a trumpet-like profile. A nonhomogeneous diameter is obviously detrimental for photonic crystals. The same authors have polished the surface of the sample after laser processing to obtain highly homogeneous nanostructures [127].
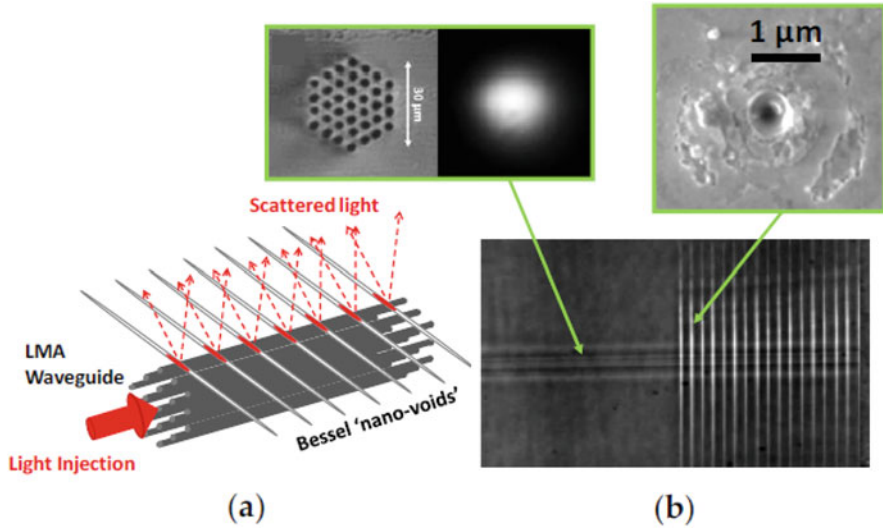
Fig. 16.12 Concept (left) and images of a photonic crystal waveguide structure inside chalco-genide glass (top images). The Bessel-induced nanovoids are used as scattering centers to couple light out of the waveguide. Reprinted figure with permission from [123]

4.5 Drilling and Cutting of Glass and Sapphire

High-speed cutting and drilling of glass are essential for a large number of mass fabrication applications, particularly in the field of microelectronics and consumer electronics. The need is to drill and/or separate glass sheets with a thickness comprised between some tens to several hundred micrometers. The resistance of glass should be preserved; it should be free of chipping with limited number of defects in the vicinity of the cut surface.

4.5.1 Drilling

It has been recently demonstrated that Bessel beams allow for cutting the whole thickness of glass slide, by translating the Bessel beam onto a trajectory while the beam is positioned such as to cross both front and exit surfaces. With this strategy, it was possible to obtain non-tapered, vertical walls for cutting of contours and opening, in transparent materials, circular holes of several tens of micrometers in diameter. An example of diamond drilling is presented in Fig. 16.13. Noticeably, the burst regime, although improving the ablation rate, is not always the best option to obtain the highest quality structures [128–130]. An improvement of the ablation efficiency can be obtained using double pulses with a typical delay of 50 ps, which corresponds to the lifetime of self-trapped excitons [114] (in this case, the
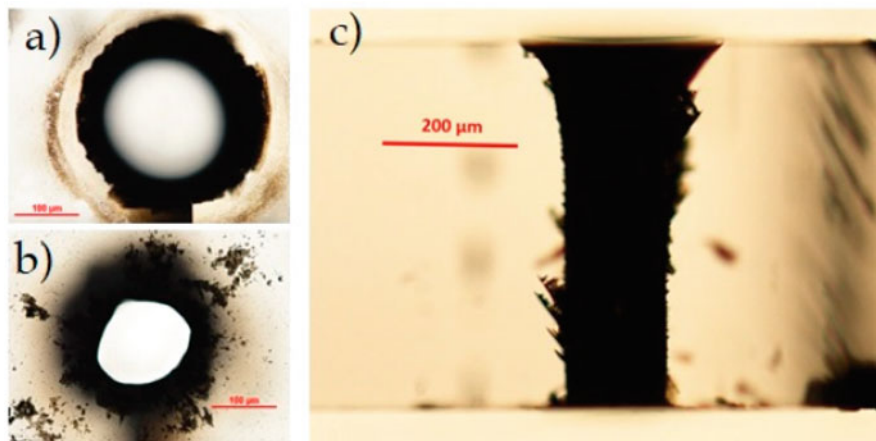
Fig. 16.13 Characterization by optical microscopy of a through-hole drilled inside 500 μm-thick diamond, using 100 writing circles. (**a**) Top, (**b**) bottom, and (**c**) lateral views. Reprinted figure with permission from [130]

pulse energy is usually lower than the one needed to open a void in single shot). An alternative approach to linear beam shaping is to produce, by nonlinear pulse propagation into a water film flowing on a workpiece, a filament, which is then used to process the workpiece. Water also contributes to material removal [131].

To increase the ablation removal rate while drilling high aspect ratio craters in glass, Ito et al. have used the superposition of a femtosecond laser filament to a continuous-wave beam at 1064 nm wavelength [132, 133]. The free electrons generated inside the filament absorb the continuous laser light efficiently. The high amount of energy absorbed over a cylinder inside glass opens an ablation crater with a diameter of 10 μm and a length of ∼130 μm in 40 ms .

4.5.2   Transparent Material Separation Without Ablation: Stealth Dicing

Stealth dicing of glass is probably one of the most important commercial applications of ultrafast lasers in the last decade. Although the material to separate is at millimeter thickness scale, it is the control of laser-induced nanometric modifications that enable a drastically new regime of separation. Stealth dicing was initially developed to cut silicon wafers at high speed [134]. It consists of generating a plane of defects within the depth of a brittle material to cut and, in a second step, of applying a stress such that a fracture propagates through the defects and cleaves the workpiece. In the initial technology, the laser was a nanosecond infrared source, and the modifications in silicon were extending over some tens of micrometers.

A similar technique was developed by Ahmed et al. for glass separation with micrometric resolution [58, 136]. In this case, the modifications were based
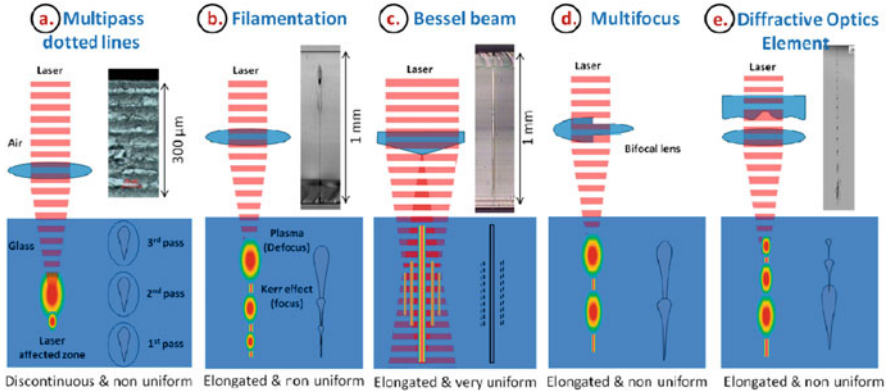
Fig. 16.14 Different strategies for ultrafast laser inscription of modifications inside glass for stealth dicing. Reprinted figure with permission from [135]

on the filamentation of ultrashort pulses. Figure 16.14 compares different types of modifications tested to reach high-speed and high-quality cutting. A typical separation between the high aspect ratio voids is ∼5–25µm, such that a laser source with repetition rate of several 100s kHz allows for processing glass at a speed on the order of 1 m/s. Apart from speed, the benefit is the quasi-absence of dust particles since it is not really an ablative process. The kerf is zero and, in optimal conditions, the method is free from chipping.

First implementations of Bessel beams in this field were performed by Tsai [137] and Bhuyan [138]. The main benefit is to produce a highly homogeneous stress distribution along the material thickness, which is crucial to maintain a high cut quality for tempered glass [138]. In this reference, the authors demonstrated from mechanical cleaving that the optimal beam position was fully inside the sample and used single pulses with a pulse duration of 11 ps. Cutting was achieved at a speed of 270 mm/s.

Overall, the cutting can be along straight or curved paths [80], and the surface quality is conventionally relatively rough (typ. between 0.5 µm and several µm). It is highly linked to the extension of internal cracks [67] and therefore to the illumination parameters as described in [135]. Particularly, the use of bursts and thermal load can benefit to the cleaving operation [80] but requires fine adjustment, for instance, using a dash line strategy [135].

As for the second step, the cleaving operation, several approaches were used: most research groups used mechanical flexure, whereas CO_2 laser provides highly repeatable conditions [67, 139]; it can be also noted that tempered glass is internally stressed by the chemical treatment such that it self-cleaves.

Although the stealth dicing technology has promptly emerged and attracted the interest of a large number of research groups and companies, only few publications quantitatively compared the different techniques. Li et al. compared filamentation-based cleaving of glass to laser surface scribing and to combinations of filamentation

and V-groove scribing, against a number of criteria: cleaving guidance, reproducibility, breaking force, morphology of the cut surface, and flexural strength of the cut parts. Using a single-pulse filamentation, the assistance of a V-groove was found to improve the cutting quality. Overall, the best results were found for a burst-mode filamentation, when the filament is formed fully inside the 1 mm-thick glass sample. The authors reported submicron roughness of the cleaved facets, with the nicest edges and a flexural strength nearly equal to the pristine reference material [140]. Dudutis et al. quantitatively compared Bessel beam-based stealth dicing using sub-picosecond pulses with more conventional glass cutting techniques such as laser-based rear-side machining, mechanical scribe and cleave, water jet cutting, or diamond saw cutting [141]. Their analysis also involved a number of criteria, including residual stress. The Bessel beam approach provided the results with the less residual surface cracks and chipping. Yet as the flexural strength of the cut samples is less than for conventional rear-side machining, the regime of pulse duration and energy used here with the Bessel beam creates a large heat-affected zone and cracks extending over several tens of micrometers, which are very likely fragilizing the cut material. Shorter pulse durations tend to minimize the damaged region. One can remark that the procedure used to apply the stress that separates the samples appears to be an important parameter although the field is yet lacking of published studies.

4.5.3 Thick Glass Cutting

Most of the previously mentioned work dealt with the cutting of relatively thin flat glass sheets, with thickness ranging from 30 μm to approximately 2 mm, because the typical Bessel zone or filament length is on the order of 200–700 μm. Cutting of multi-mm-thick glass requires other strategies. A first approach is to generate multiple modification surfaces, on top of each other to cover most of the glass thickness in multiple passes. This approach obviously decreases the overall process throughput and requires a fine alignment of the planes written on top of each other, which needs high repeatability translation stages.

A second approach is to extend the Bessel zone length to multi-millimeter scale so as to enable cutting using a single-laser pass. Extending the beam length using the same cone angle imposes to increase the pulse energy in the same ratio as the length increase. For multi-mm-long ranges, the burst energy should be on the order of 1 mJ. It is difficult to use such energy in the conventional telescopic setup used to magnify the cone angle (see Sect. 2.1) mostly because of the risk of optical damage to the second lens. Indeed, as the Bessel zone extends, its Fourier transform is thinner, with a much higher energy than for the processing of thin samples. To avoid the use of the 2f-2f setup, high apex angle axicons were used to shape the ultrafast laser beam.

To increase the working distance to several millimeters, the three-axicon shaping technique of reference [26] was implemented to produce 8 mm-long modifications in glass [142]. (One can remark that in [143], a single axicon is used, with obvious

limitation on the working distance, but mJ pulses used enabled cutting 8 mm glass in single pass.) The setup was slightly improved using a pair of negative and positive axicons to avoid any intermediate hotspots or focusing [27] (see Sect. 2). With this approach, extremely thick glass, up to 1 cm thickness, could be cleaved using the stealth dicing technique [27]. Noticeably, the aspect ratio of the nanovoids, using the same geometry, has been scaled from 100:1 in [8] to 30,000:1 in [27]. Very thick glass cutting opens new opportunities to reduce costs for window glass processing in a context where better insulating windows are required to limit our carbon footprint.

5 Perspectives

Thick and thin glass processing using diffraction-free Bessel beams has been very active in the recent years. Even more recently, a number of new orientations have attracted attention. It was realized that shaping the central lobe of the Bessel beam could enhance the performances of stealth dicing. The stealth dicing technique has also been widened to curved glass cutting. New strategies are being developed to cut glass with curved surface in a single pass, and finally, the family of Bessel beams has been generalized to create almost arbitrary transverse cross sections that propagate preserving the conical flow and longitudinal invariance.

5.1 *Crack Formation*

Micro-crack formation seems to be the mechanism allowing material separation where the stress-induced fracture propagates through the laser-induced crack network. The transient stress and crack propagation imaging has been reported in [144, 145]. Cracks with a transverse extension of several tens of micrometers can be produced using high-energy pulses, particularly when using relatively long pulse duration. Increasing the crack extent allows for increasing the channel to channel distance and, while this increases the surface roughness, straightforwardly improves the process speed.

In sapphire, cracks can be generated following the crystal axes. Rapp et al. demonstrated that using approximately ten times the energy needed to produce a nanochannel in single shot, cracks extending over ~ 20 µm were generated in a star-shape following the three axes of the hexagonal lattice [83]. Interestingly, below a pulse duration of ~ 600 fs, only a single crack is generated, perpendicular to the polarization axis. This can be understood from the elliptical transverse shape of the nanovoid formed in the femtosecond regime (see Sect. 3.5). Polarization could then be used to control the crack direction, although a nontrivial coupling exists with the stress induced by formerly drilled nanochannels. These results were also confirmed in reference [146], in which cutting of sapphire along a curved path is demonstrated at 500 mm/s (see Fig. 16.15).
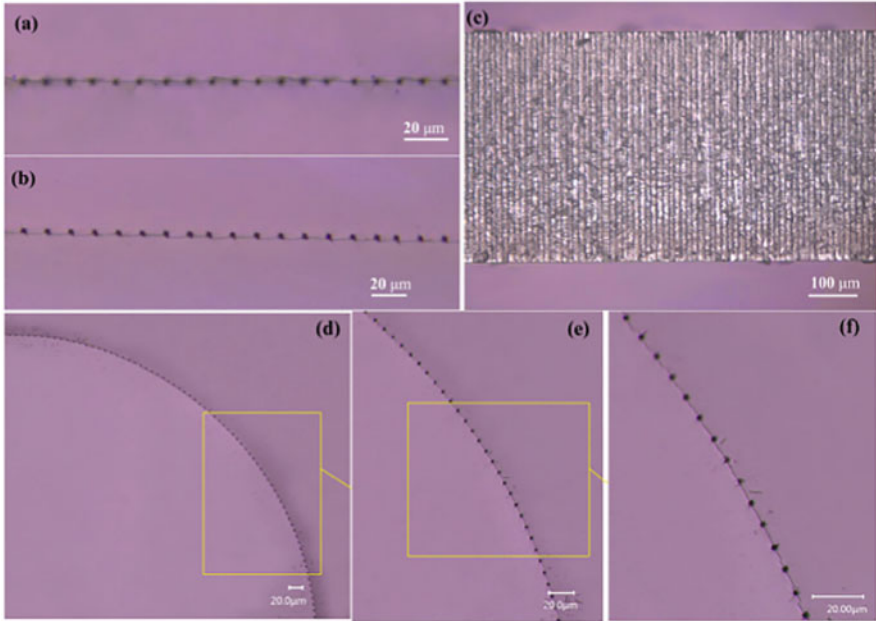
Fig. 16.15 Control of the formation of cracks after Bessel beam illumination. The cutting speed is 0.5 m/s. The images show optical microscopy characterization of the sample. (**a**, **b**) Top and bottom views before cleavage of a line-type modification. (**c**) View of the cleaved surface of the line-type modification. (**d–f**) Top views of a curvilinear cleave with different magnifications. The radius of curvature is 500 μm. Reprinted figure with permission from [146]

In glass, the transverse cross section of the channels does not show any ellipticity. This can be controlled using a specific beam shape, for instance, by producing an elliptical Bessel beam, formed by filtering part of the intensity ring distribution in the Fourier space [147] or by using more complex beam shaping approaches [148, 149] or simply using imperfect axicons or an axicon with a tilt [21, 150, 151]. The elliptical cross section of the channels increases the stress along the major axis of the ellipse. This improves the cleavability of the material and the flexural strength of the cut material [152]. Another similar approach using multiple cavities has been suggested and modeled in reference [153].

Another way of controlling the crack formation and improving the process throughput is the use of a dash line strategy where groups of channels are processed and a crack joins the groups during material separation. This strategy improves guiding the overall fracture, particularly for the separation of materials cut along curved paths [135].
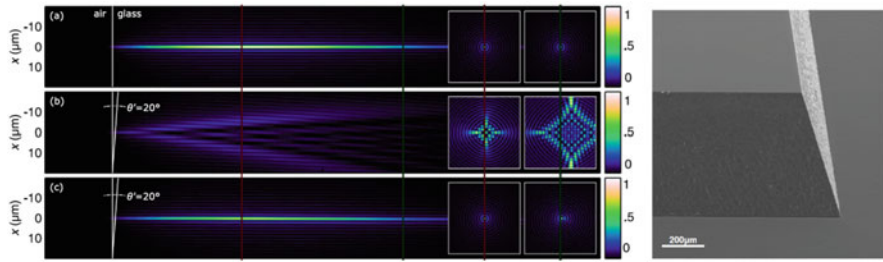
Fig. 16.16 (left) Simulation of Bessel beam intensity distribution inside glass: (**a**) if the glass surface is normal to the beam axis, (**b**) if the surface is tilted by 20°, (**c**) same as (**b**) but the Bessel beam is pre-corrected. (Right) Example of glass cutting with a tilt of 30° with respect to the normal. Reprinted figure with permission from [154]. Copyright The Optical Society

5.2 Aberration Correction for Non-flat Glass Cutting

The applications of glass cutting are by far limited to neither flat glass nor vertical cutting. Glass vertically cut at 90° from its surface can undergo chipping or breaking when handled because of stress accumulation at the corners. However, the beam inclination that is necessary to create beveled edges induces a strong beam distortion, as can be observed from Fig. 16.16 (middle left). The subsequent intensity drop within the beam prevents nanochannel drilling. Jenne et al. compensated the aberration due to the inclined glass surface using a phase mask computed with a decomposition of the aberration on Zernike polynomials [154]. Successful cutting with 30° tilt angle is shown in Fig.16.16 (right). A more precise aberration correction was developed in reference [139], where the aberration is computed by inverse propagation. In this reference, the phase mask is additionally engineered to produce an elliptical Bessel beam.

A similar problem arises to cut curved surfaces such as glass tubes for ampoules or syringes. Flamm et al. applied a quadratic phase compensation to preserve the shape of the Bessel beam inside a curved glass article. Figure 16.17 compares the beam intensity distribution produced within glass without and with the aberration correction. Obviously, the correction is dependent on the curvature of the article [155].

The cut parts of the tube shown in Fig. 16.17 have been removed using laser illumination with the corrected Bessel beam and chemical etching. This overall demonstrates the usefulness and flexibility of laser structuring using non-diffracting Bessel beams.
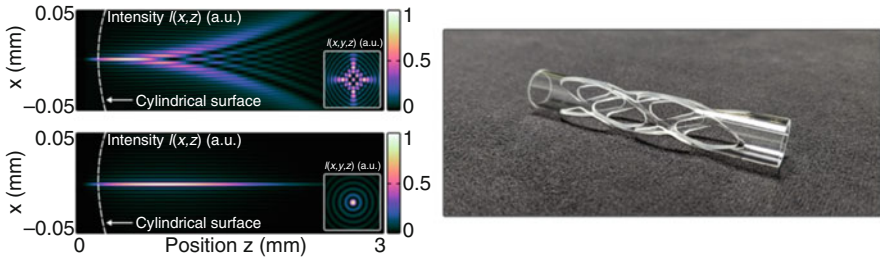
Fig. 16.17 (left) Simulation of Bessel beam intensity distribution inside curved glass, before (top) and after correction (bottom). (Right) Complex contour cutting from a glass tube. Etching is used after laser illumination to enable material removal. Reprinted figure with permission from [155]

5.3 Laser Processing of Curved Structures

This section discusses the application to edge chamfering that is necessary for glass handling and reducing the stress accumulation within the corners, as mentioned in Sect. 5.2. Instead of the three passes at three different angles that are necessary to cut and chamfer glass in a bull-nose shape, it would be desirable to have a process performing this operation in a single step. A fully curved profile would even more reduce the stress confinement due to sharp angles. In this context, other classes of extended beams, i.e., accelerating beams and, in more general, beams with a curvature, can offer new opportunities.

Self-accelerating beams are beams which produce an interference pattern that laterally shifts along a curve during propagation. A first version, the "Airy beam," was produced using a third-order phase and an optical Fourier transformation [156]. It was early used to produce curved plasma channels in air [157, 158]. By recognizing that accelerating beams are caustics, it is in fact possible to largely extend the self-acceleration property to arbitrary curved trajectories, which can even extend to the non-paraxial regime [159–164].

First applications to curved laser micromachining were developed by Mathis et al. where accelerating beams were used for edge polishing and curved trench opening [163, 165] and to inscribe a curved damage inside glass [161]. A challenging issue in the field is the generation of curvatures with large radius. This requires very large extents of the third-order phase applied in the Fourier plane as well as optics with large pupils: the beams developed by Mathis et al. could be curved only over a distance of typically 50 to 70 μm while reaching a tilt of $\pm \sim 45°$ (see Fig. 16.18 (left) [163]). Recently, using a similar approach, Sohr et al. demonstrated curved modifications of 700 μm glass that could be etched, with a maximal tilt of $\sim 18°$, as shown in Fig. 16.18 (right) [166].

To circumvent the abovementioned difficulty of phase extent to create an accelerating beam with large maximal tilt to process glass with thickness of several hundreds of micrometers to millimeters, a new strategy was developed in [167].
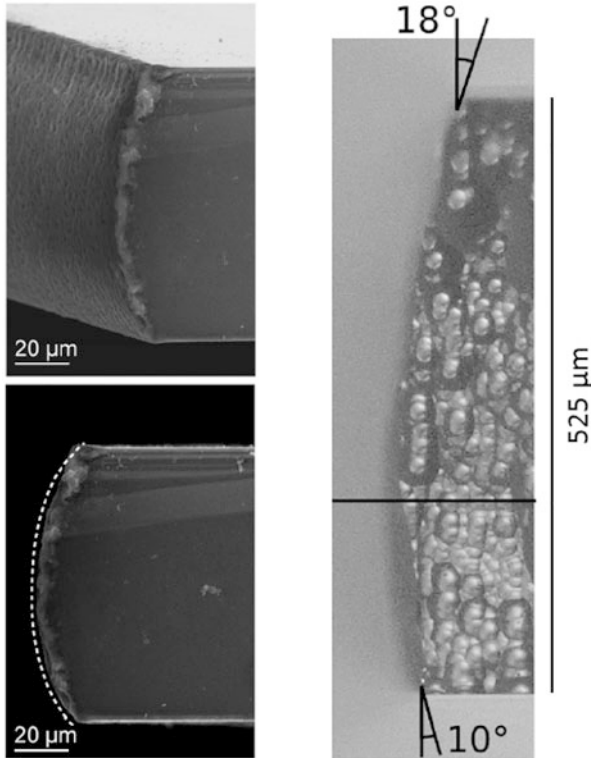
Fig. 16.18 (left) Curved edge processing of 50 μm-thick silicon using an accelerating beam. Reprinted figure with permission from [163]; (right) two-step curved edge processing in glass: laser illumination using an accelerating beam is used before chemical etching to enable material separation. Reprinted and adapted figure with permission from [166]. Copyright The Optical Society

The concept, as shown in Fig. 16.19, is to generate a series of focii positioned on a curved trajectory. Very large tilt angles can be reached as can be seen in Fig. 16.19 (right).

5.4   Bessel-Like Beams and Applications

Most of the works discussed up to here were based on zeroth-order Bessel beams. However, it is easy to understand that higher-order Bessel beams or other beam shapes could offer interesting perspectives in the field of laser micromachining and nanomachining.

Jukna et al. demonstrated that higher-order Bessel beams can sustain—if the cone angle is sufficiently high—the same propagation-invariant regime as the one
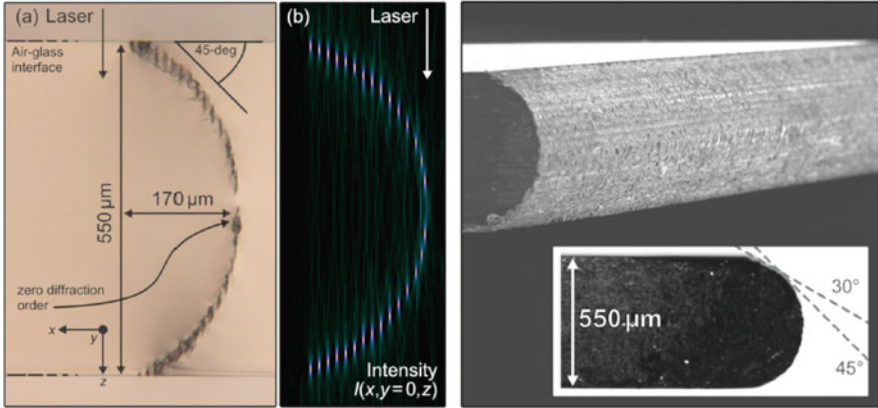
Fig. 16.19 Curved edge processing using a series of focii distributed over a half-circle. Material separation is obtained after chemical etching. Reprinted figure with permission from [167]

generated by zeroth-order Bessel beams [168]. Higher-order Bessel beams have been tested by several groups for laser processing. However, a key aspect is that at the high power necessary to induce material modification, the cone angle generally used can be insufficient to prevent nonlinear modulation instability. It tends to split the main intensity ring [169]. As shown in [170], the main ring of the higher-order Bessel can split into multiple hotspots during the propagation. Jedrkiewicz et al. reported single-shot induced tubular modifications in glass using higher-order Bessel beams in the picosecond regime [171]. In the femtosecond regime, modifications are visible only at the surface. In reference [172], azimuthal and radial polarizations of a first-order Bessel beam have been compared in the context of picosecond laser crack formation inside glass. It was shown the most prominent effect is in fact the intensity asymmetries of the beam.

A new class of Bessel-like beams has been introduced by Jenne et al. with a generalization of the azimuthal phase applied [148, 149]. The phase of an nth-order Bessel beam is, in radial coordinates(r, φ):

$$\Psi(r, \varphi) = \frac{2\pi}{\lambda} \sin \gamma r + n\varphi \tag{16.3}$$

This generates a beam with a transverse intensity profile close to $|J_n(r)|^2$ function. The first term is responsible for the conical structure of the beam, while the second determines the transverse position of the intensity maxima, since they are the points of constructive interference. The concept introduced by Jenne and Flamm is to modify the second term, following [148, 149]:

$$\Psi(r, \varphi) = \frac{2\pi}{\lambda} \sin \gamma r + \Theta(\varphi) \tag{16.4}$$
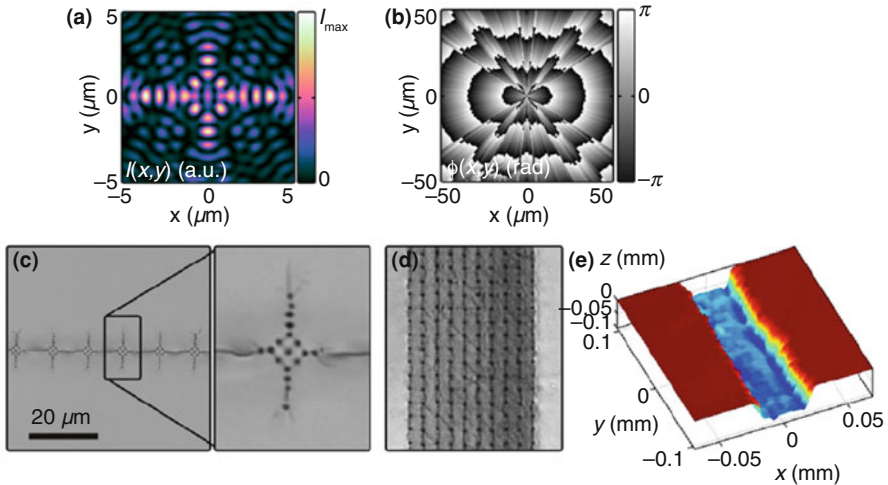
Fig. 16.20 (**a**) Cross section of a Bessel-like beam generated using the phase mask shown in (**b**). (**c**) SEM view of a series of ultrafast laser-induced material modifications and cracks using the beam shape (**a**). (**d**) After scanning the beam over a series of lines, a square array of cracks and channels is created. (**e**) shows the profile of a trench after chemical etching of the sample shown in (**d**). Reprinted figure with permission from [155]

where Θ is an arbitrary function. With this approach, the group developed beam shapes that can efficiently control the formation of well-oriented extended cracks. The use of asymmetrically shaped central lobe of Bessel beam [149] confirms the results of Meyer et al. [152].

Figure 16.20 demonstrates that Bessel-like shaping opens a very large number of possibilities to engineer the stress distribution inside glass, obviously not limited to glass cleaving applications.

Other approaches have also been used to engineer Bessel beams while preserving their non-diffracting properties, such as superpositions of laterally shifted Bessel vortices [173], superpositions of vortices [174], or the synthesis of non-diffracting Mathieu and Weber beams [175]. Using superimposed vortex orders, Yu et al. reduced the intensity of the side lobes which was successfully applied to surface nanostructuring with reduced limitation on the fluence in the central peak, as shown in Fig. 16.21 [176].

6   Conclusion

As a conclusion, ultrafast laser beam shaping as quasi-diffraction-free Bessel beams that propagate in a conical flow has enabled the development of drastically new laser nanostructuring applications, down to the extreme regime of 100 nm laser
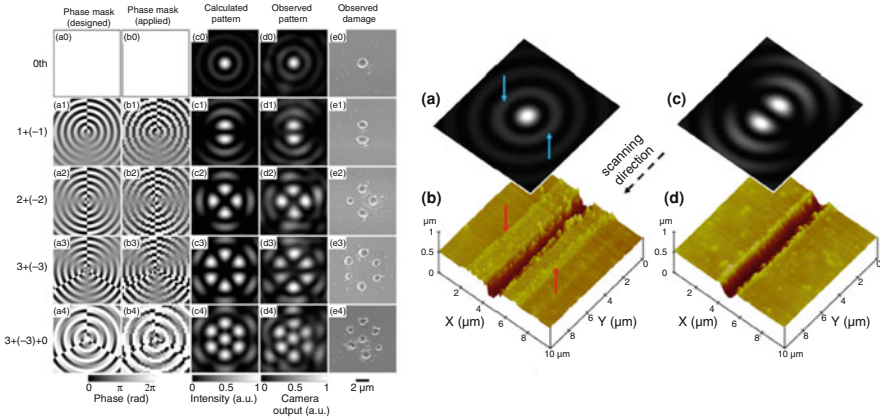
Fig. 16.21 (left) Superpositions of different Bessel beams leads to multiple spots and can be used to process material surface; (right) trench nanomachining using an engineered Bessel-like beam can reduce the damage produced by side lobes. Reprinted figure with permission from [176]

structuring and extremely high aspect ratio up to 30,000 to 1. The strength of the approach is that these extreme scales are also very well adapted for real-life technological applications. The very long focal region of Bessel beams releases the constraint on ultraprecise sample positioning when nanostructuring, non-flat surfaces can be processed. Inside solids, the laser beam shaping enables the generation of extended index modification, photopolymerization, or void formation with applications in photonics or to high-speed thin or thick glass cutting. This chapter has also reviewed recent new directions of the field where new beam shapes are being developed, maintaining the conical flow property, but where the transverse intensity distribution is engineered to control targeted effects with enhanced transverse directionality. The recent generalization of Bessel beams and the development of non-diffracting caustics [177] open a new toolbox to control matter at extreme scales and extreme regimes with ultrafast laser pulses.

It is no doubt that next generation of very high-power, kilowatt-class lasers will offer new opportunities for further developments since the extended focus of Bessel and Bessel-like beams requires more energy and higher average power [178]. On a fundamental side, the nanometric scale of the laser-induced plasmas inside dielectrics still represents a challenge for the laser-matter interaction in this regime, but recent results make us oversee that extreme states can be reached using these beam shapes with both fundamental and technological impacts. Warm dense matter can be generated over extremely long distances using only a tabletop laser, in contrast with much more complex high-energy sources currently used. On the technological aspects, the extreme pressures and temperatures reached within the materials over lengths at centimeter-scale can offer also very interesting perspectives in terms of new material synthesis [179].

References

1. J. Durnin, J.J. Miceli, J.H. Eberly, Diffraction-free beams. Phys. Rev. Lett. **58**, 1499–1501 (1987)
2. M. Duocastella, C. Arnold, Bessel and annular beams for materials processing. Laser Photon. Rev. **6**, 607–621 (2012)
3. F. Courvoisier, R. Stoian, A. Couairon, Ultrafast laser micro- and nano-processing with nondiffracting and curved beams. Opt. Laser Technol. **80**, 125–137 (2016)
4. R. Stoian, M.K. Bhuyan, G. Zhang, G. Cheng, R. Meyer, F. Courvoisier, Ultrafast Bessel beams: advanced tools for laser materials processing. Adv. Opt. Technol. **7**, 165–174 (2018)
5. R. Stoian, Volume photoinscription of glasses: three-dimensional micro- and nanostructuring with ultrashort laser pulses. Appl. Phys. A Mater. Sci. Process. **126**, 438 (2020)
6. F. Courvoisier, Ultrafast laser micro-nano structuring of transparent materials with high aspect ratio, in *Handbook of Laser Micro- and Nano-Engineering* (Springer International Publishing, 2020), pp. 1–37
7. V. Jarutis, R. Paškauskas, A. Stabinis, Focusing of Laguerre–Gaussian beams by axicon. Optics Communications **184**, 105–112 (2000)
8. M.K. Bhuyan, F. Courvoisier, P.A. Lacourt, M. Jacquot, R. Salut, L. Furfaro, J.M. Dudley, High aspect ratio nanochannel machining using single shot femtosecond Bessel beams. Appl. Phys. Lett. **97**, 081102 (2010)
9. J.H. McLeod, The axicon: A new type of optical element. J. Opt. Soc. Am. **44**, 592 (1954)
10. L. Froehly, M. Jacquot, P.A. Lacourt, J.M. Dudley, F. Courvoisier, Spatiotemporal structure of femtosecond Bessel beams from spatial light modulators. J. Opt. Soc. Am. A **31**, 790 (2014)
11. P. Brandão, D. Pires, Transmission and reflection of vector Bessel beams through an interface between dielectrics. Phys. Lett. A **381**, 813–816 (2017)
12. N. Chattrapiban, E.A. Rogers, D. Cofield, I. Wendell T. Hill, R. Roy, Generation of nondiffracting Bessel beams by use of a spatial light modulator. Optics Letters **28**, 2183 (2003)
13. A. Vasara, J. Turunen, A.T. Friberg, Realization of general nondiffracting beams with computer-generated holograms. J. Opt. Soc. Am. A **6**, 1748 (1989)
14. J. Amako, D. Sawaki, E. Fujii, Microstructuring transparent materials by use of nondiffracting ultrashort pulse beams generated by diffractive optics. J. Opt. Soc. Am. B **20**, 2562 (2003)
15. S.N. Khonina, V.V. Kotlyar, R.V. Skidanov, V.A. Soifer, K. Jefimovs, J. Simonen, J. Turunen, Rotation of microparticles with Bessel beams generated by diffractive elements. J. Modern Opt. **51**, 2167–2184 (2004)
16. R. Grunwald, U. Neumann, V. Kebbel, H.J. Kühn, K. Mann, U. Leinhos, H. Mischke, D. Wulff-Molder, Vacuum-ultraviolet beam array generation by flat micro-optical structures. Optics Letters **29**, 977 (2004)
17. T. Grosjean, S.S. Saleh, M.A. Suarez, I.A. Ibrahim, V. Piquerey, D. Charraut, P. Sandoz, Fiber microaxicons fabricated by a polishing technique for the generation of Bessel-like beams. Applied Optics **46**, 8061 (2007)
18. X. Tsampoula, V. Garceés-Chavez, M. Comrie, D.J. Stevenson, B. Agate, C.T.A. Brown, F. Gunn-Moore, K. Dholakia, Femtosecond cellular transfection using a nondiffracting light beam. Appl. Phys. Lett. **91**, 053902 (2007)
19. S. Akturk, B. Zhou, M. Franco, A. Couairon, A. Mysyrowicz, Generation of long plasma channels in air by focusing ultrashort laser pulses with an axicon. Optics Communications **282**, 129–134 (2009)

20. P. Boucher, J.D. Hoyo, C. Billet, O. Pinel, G. Labroille, F. Courvoisier, Generation of high conical angle Bessel–Gauss beams with reflective axicons. Applied Optics **57**, 6725 (2018)
21. J. Dudutis, P. Gečys, G. Račiukaitis, Non-ideal axicon-generated Bessel beam application for intra-volume glass modification. Optics Express **24**, 28433 (2016)
22. O. Brzobohatý, T. Cižmár, P. Zemánek, High quality quasi-Bessel beam generated by round-tip axicon. Optics Express **16**, 12688 (2008)
23. T. Čižmár, K. Dholakia, Tunable Bessel light modes: engineering the axial propagation. Optics Express **17**, 15558 (2009)
24. S. Schwarz, G.L. Roth, S. Rung, C. Esen, R. Hellmann, Fabrication and evaluation of negative axicons for ultrashort pulsed laser applications. Optics Express **28**, 26207 (2020)
25. S. Schwarz, S. Rung, C. Esen, R. Hellmann, Rapid fabrication of precise glass axicon arrays by an all laser-based manufacturing technology. J. Laser Appl. **32**, 012001 (2020)
26. B. Chebbi, S. Minko, N. Al-Akwaa, I. Golub, Remote control of extended depth of field focusing. Optics Communications **283**, 1678–1683 (2010)
27. R. Meyer, L. Froehly, R. Giust, J.D. Hoyo, L. Furfaro, C. Billet, F. Courvoisier, Extremely high-aspect-ratio ultrafast Bessel beam generation and stealth dicing of multi-millimeter thick glass. Appl. Phys. Lett. **114**, 201105 (2019)
28. I. Ouadghiri-Idrissi, R. Giust, L. Froehly, M. Jacquot, L. Furfaro, J.M. Dudley, F. Courvoisier, Arbitrary shaping of on-axis amplitude of femtosecond Bessel beams with a single phase-only spatial light modulator. Optics Express **24**, 11495–11504 (2016)
29. R. Dharmavarapu, S. Bhattacharya, S. Juodkazis, Diffractive optics for axial intensity shaping of Bessel beams. J. Opt. (UK) **20**, 085606 (2018)
30. P. Gotovski, P. Šlevas, E. Nacius, V. Jukna, S. Orlov, J. Baltrukonis, O. Ulčinas, T. Gertus, Formation of optical needles by Pancharatnam-Berry phase element for laser-induced modifications in transparent materials, in *Laser-based Micro- and Nanoprocessing XIV*, vol. 11268, ed. by U. Klotzbach, A. Watanabe, R. Kling (International Society for Optics and Photonics (SPIE), 2020), pp. 357–365
31. A.P. Joglekar, H. h. Liu, E. Meyhofer, G. Mourou, A.J. Hunt, Optics at critical intensity: Applications to nanomorphing. Proc. Natl. Acad. Sci. **101**, 5856–5861 (2004)
32. R. Sahin, I. Kabacelik, Nanostructuring of ito thin films through femtosecond laser ablation. Appl. Phys. A Mater. Sci. Process. **122**, 314 (2016)
33. D.H. Doan, R. Iida, B. Kim, I. Satoh, K. Fushinobu, Bessel beam laser-scribing of thin film silicon solar cells by ns pulsed laser. J. Thermal Sci. Technol. **11**, 11 (2016)
34. B. Wetzel, C. Xie, P.A. Lacourt, J.M. Dudley, F. Courvoisier, Femtosecond laser fabrication of micro and nano-disks in single layer graphene using vortex Bessel beams. Appl. Phys. Lett. **103**, 241111 (2013)
35. B. Voisiat, M. Gedvilas, S. Indrišiūnas, G. Račiukaitis, Picosecond-laser 4-beam-interference ablation as a flexible tool for thin film microstructuring. Physics Procedia **12**, 116–124 (2011)
36. S. Alamri, A.F. Lasagni, Development of a general model for direct laser interference patterning of polymers. Optics Express **25**, 9603 (2017)
37. X. Li et al., Creating a three-dimensional surface with antireflective properties by using femtosecond-laser Bessel-beam-assisted thermal oxidation. Optics Letters **45**, 2989 (2020)
38. I. Alexeev, K.H. Leitz, A. Otto, M. Schmidt, Application of Bessel beams for ultrafast laser volume structuring of nontransparent media. Physics Procedia **5**, 533–540 (2010)
39. Y. Matsuoka, Y. Kizuka, T. Inoue, The characteristics of laser micro drilling using a Bessel beam. Appl. Phys. A Solids Surf. **84**, 423–430 (2006)
40. O. Jedrkiewicz et al., Pulsed Bessel beam-induced microchannels on a diamond surface for versatile microfluidic and sensing applications. Opt. Mater. Exp. **7**, 1962 (2017)
41. S. Kumar et al., Laser surface structuring of diamond with ultrashort Bessel beams. Scientific Reports **8**, 14021 (2018)
42. H.D. Nguyen et al., Non-diffractive Bessel beams for ultrafast laser scanning platform and proof-of-concept side-wall polishing of additively manufactured parts. Micromachines **11**, 974 (2020)

43. A. Couairon, A. Mysyrowicz, Femtosecond filamentation in transparent media. Physics Reports **441**, 47–189 (2007)
44. P. Polesana, M. Franco, A. Couairon, D. Faccio, P.D. Trapani, Filamentation in Kerr media from pulsed Bessel beams. Phys. Rev. A **77**, 043814 (2008)
45. E. Gaizauskas et al., Discrete damage traces from filamentation of Gauss-Bessel pulses. Optics Letters **31**, 80 (2006)
46. I. Ouadghiri-Idrissi, J.M. Dudley, F. Courvoisier, Controlling nonlinear instabilities in Bessel beams through longitudinal intensity shaping. Optics Letters **42**, 3785 (2017)
47. I. Ouadghiri-Idrissi, J.M. Dudley, F. Courvoisier, Control of spatial four-wave-mixing efficiency in Bessel beams using longitudinal intensity shaping. Phys. Rev. A **100**, 043804 (2019-10)
48. V. Garzillo et al., Optimization of laser energy deposition for single-shot high aspect-ratio microstructuring of thick BK7 glass. J. Appl. Phys. **120**, 013102 (2016)
49. P.K. Velpula, M.K. Bhuyan, C. Mauclair, J.P. Colombier, R. Stoian, Role of free carriers excited by ultrafast Bessel beams for submicron structuring applications. Optical Engineering **53**, 076108 (2014)
50. L. Sudrie et al., Femtosecond laser-induced damage and filamentary propagation in fused silica. Phys. Rev. Lett. **89**, 4135 (2002)
51. S. Tzortzakis et al., Self-guided propagation of ultrashort IR laser pulses in fused silica. Phys. Rev. Lett. **87**, 213902 (2001)
52. R. Beuton et al., Numerical studies of dielectric material modifications by a femtosecond Bessel–Gauss laser beam. Appl. Phys. A Mater. Sci. Process. **127**, 334 (2021)
53. K. Ardaneh et al., A new route to high energy density inside the bulk of transparent materials (2021). arXiv:2109.00803
54. D. Faccio et al., Kerr-induced spontaneous Bessel beam formation in the regime of strong two-photon absorption. Optics Express **16**, 8213 (2008)
55. L. Luo et al., Formation of diversiform microstructures in wide-bandgap materials by tight-focusing femtosecond laser pulses. J. Opt. A Pure Appl. Optics **4**, 105–110 (2001)
56. S. Sowa, W. Watanabe, J. Nishii, K. Itoh, Filamentary cavity formation in poly(methyl methacrylate) by single femtosecond pulse. Appl. Phys. A **81**, 1587–1590 (2005)
57. J. Song et al., Formation mechanism of self-organized voids in dielectrics induced by tightly focused femtosecond laser pulses. Appl. Phys. Lett. **92**, 092904 (2008)
58. F. Ahmed, M.S. Ahsan, M.S. Lee, M.B.G. Jun, Near-field modification of femtosecond laser beam to enhance single-shot pulse filamentation in glass medium. Appl. Phys. A **114**, 1161–1165 (2013)
59. E. Alimohammadian, E. Ertorer, E.M. Uzeda, J. Li, P.R. Herman, Inhibition and enhancement of linear and nonlinear optical effects by conical phase front shaping for femtosecond laser material processing. Scientific Reports **10**, 21528 (2020)
60. E. Alimohammadian, E. Ertorer, P.R. Herman, Conical phase front and aberration beam shaping for manipulating femtosecond laser chemical etching. Opt. Mater. Exp. **11**, 2432 (2021)
61. P.K. Velpula et al., Spatio-temporal dynamics in nondiffractive Bessel ultrafast laser nanoscale volume structuring. Laser Photon. Rev. **10**, 230–244 (2016)
62. R. Stoian, M.K. Bhuyan, A. Rudenko, J.P. Colombier, G. Cheng, High-resolution material structuring using ultrafast laser non-diffractive beams. Adv. Phys. X **4**, 1659180 (2019)
63. A. Marcinkevicius, S. Juodkazis, S. Matsuo, V. Mizeikis, H. Misawa, Application of Bessel beams for microfabrication of dielectrics by femtosecond laser. Jpn. J. Appl. Phys. **40**, L1197–L1199 (2001)
64. V. Zambon, N. McCarthy, M. Piché, Fabrication of photonic devices directly written in glass using ultrafast Bessel beams, in R. Vallée, et al. (eds.) *Photonics North 2008*, vol. 7099 (International Society for Optics and Photonics (SPIE), 2008), pp. 720–724
65. S. Juodkazis et al., Laser-induced microexplosion confined in the bulk of a sapphire crystal: Evidence of multimegabar pressures. Phys. Rev. Lett. **96**, 166101 (2006)

66. S. Juodkazis, H. Misawa, T. Hashimoto, E.G. Gamaly, B. Luther-Davies, Laser-induced microexplosion confined in a bulk of silica: Formation of nanovoids. Appl. Phys. Lett. **88**, 201909 (2006)
67. F. Werr et al., Surface probing of ultra-short-pulse laser filament cut window glass and the impact on the separation behavior. Adv. Eng. Mater. **22**, 2000471 (2020)
68. N. Götte et al., Temporal Airy pulses for controlled high aspect ratio nanomachining of dielectrics. Optica **3**, 389 (2016-04)
69. S. Winkler et al., Transient response of dielectric materials exposed to ultrafast laser radiation. Appl. Phys. A Solids Surf. **84**, 413–422 (2006)
70. L. Rapp et al., High aspect ratio micro-explosions in the bulk of sapphire generated by femtosecond Bessel beams. Scientific Reports **6**, 34286 (2016)
71. T. Chen et al., Reconstructing of embedded high-aspect-ratio nano-voids generated by ultrafast laser Bessel beams. Micromachines **11**, 671 (2020)
72. G.Y. Chang, Y.H. Wang, G.H. Cheng, Writing nanopores on a ZnS crystal with ultrafast Bessel beams. Chinese Optics **14**, 213–225 (2021)
73. C. Vetter et al., High aspect ratio structuring of glass with ultrafast Bessel beams. Materials **14**, 6749 (2021)
74. M. Lamperti et al., Invited article: Filamentary deposition of laser energy in glasses with Bessel beams. APL Photonics **3**, 120805 (2018)
75. J. del Hoyo, R. Meyer, L. Furfaro, F. Courvoisier, Nanoscale confinement of energy deposition in glass by double ultrafast Bessel pulses. Nanophotonics **10**, 1089–1097 (2020)
76. M. Garcia-Lechuga et al., Simultaneous time-space resolved reflectivity and interferometric measurements of dielectrics excited with femtosecond laser pulses. Phys. Rev. B **95**, 214114 (2017)
77. A. Denoeud et al., Metallization of warm dense SiO2 studied by XANES spectroscopy. Phys. Rev. Lett. **113**, 116404 (2014)
78. K. Engelhorn et al., Electronic structure of warm dense silicon dioxide. Phys. Rev. B **91**, 214305 (2015)
79. M. Somayaji et al., Multiscale electronic and thermomechanical dynamics in ultrafast nanoscale laser structuring of bulk fused silica. Scientific Reports **10**, 15152 (2020)
80. M. Kumkar et al., Comparison of different processes for separation of glass and crystals using ultrashort pulsed lasers, in *Frontiers in Ultrafast Optics: Biomedical, Scientific, and Industrial Applications XIV*, vol. 8972, ed. by A. Heisterkamp, P.R. Herman (International Society for Optics and Photonics (SPIE), 2014), pp. 161–176
81. K. Mishchik et al., Improved laser glass cutting by spatio-temporal control of energy deposition using bursts of femtosecond pulses. Optics Express **25**, 33271 (2017)
82. S. Karimelahi, L. Abolghasemi, P.R. Herman, Rapid micromachining of high aspect ratio holes in fused silica glass by high repetition rate picosecond laser. Appl. Phys. A **114**, 91–111 (2013)
83. L. Rapp et al., High speed cleaving of crystals with ultrafast Bessel beams. Optics Express **25**, 9312 (2017)
84. G. Zhang et al., Thermal and mechanical limitations to processing resolution in volume non-diffractive ultrafast laser structuring. Appl. Surf. Sci. **570**, 151170 (2021)
85. N.M. Bulgakova, V.P. Zhukov, S.V. Sonina, Y.P. Meshcheryakov, Modification of transparent materials with ultrashort laser pulses: What is energetically and mechanically meaningful? J. Appl. Phys. **118**, 233108 (2015)
86. K. Bergner et al., Spatio-temporal analysis of glass volume processing using ultrashort laser pulses. Applied Optics **57**, 4618 (2018)
87. T.D. Arber et al., Contemporary particle-in-cell approach to laser-plasma modelling. Plasma Phys. Controll. Fusion **57**, 113001 (2015)
88. W. Kruer, *Physics of Laser Plasma Interactions* (CRC Press, 2019)
89. N. Denisov, On a singularity of the field on an electromagnetic wave propagated in an inhomogeneous plasma. J. Exp. Theor. Phys. **4**, 544 (1957)

90. P. Stampfli, K.H. Bennemann, Dynamical theory of the laser-induced lattice instability of silicon. Phys. Rev. B **46**, 10686–10692 (1992)

91. B. Rethfeld, D.S. Ivanov, M.E. Garcia, S.I. Anisimov, Modelling ultrafast laser ablation. J. Phys. D Appl. Phys. **50**, 193001 (2017)

92. T. Winkler et al., Laser amplification in excited dielectrics. Nature Physics **14**, 74–79 (2017-09)

93. S. Mao et al., Dynamics of femtosecond laser interactions with dielectrics. Appl. Phys. A Solids Surf. **79**, 1695–1709 (2004)

94. R.G. Kraus et al., Shock vaporization of silica and the thermodynamics of planetary impact events. J. Geophys. Res. Planets **117**, E09009 (2012)

95. E.N. Glezer, E. Mazur, Ultrafast-laser driven micro-explosions in transparent materials. Appl. Phys. Lett. **71**, 882 (1997)

96. R. Beuton et al., Thermo-elasto-plastic simulations of femtosecond laser-induced structural modifications: Application to cavity formation in fused silica. J. Appl. Phys. **122**, 203104 (2017)

97. M.K. Bhuyan, P.K. Velpula, M. Somayaji, J.P. Colombier, R. Stoian, 3D nano-fabrication using controlled Bessel-glass interaction in ultra-fast modes. J. Laser Micro Nanoeng. **12**, 274–280 (2017)

98. M.K. Bhuyan et al., Ultrafast laser nanostructuring in bulk silica, a "slow" microexplosion. Optica **4**, 951 (2017)

99. M. Bonitz et al., Ab initio simulation of warm dense matter. Phys. Plasmas **27**, 042710 (2020)

100. K. Sugioka, Y. Cheng, Ultrafast lasers—reliable tools for advanced materials processing. Light Sci. Appl. **3**, e149 (2014)

101. M. Malinauskas et al., Ultrafast laser processing of materials: From science to industry. Light Sci. Appl. **5**, e16133 (2016)

102. F. Sima, K. Sugioka, Ultrafast laser manufacturing of nanofluidic systems. Nanophotonics **10**, 2389–2406 (2021)

103. M. Manousidaki, D.G. Papazoglou, M. Farsari, S. Tzortzakis, Long-scale multiphoton polymerization voxel growth investigation using engineered Bessel beams. Opt. Mater. Exp. **9**, 2838 (2019)

104. H. Cheng et al., Generation of Bessel-beam arrays for parallel fabrication in two-photon polymerization. J. Laser Appl. **33**, 012040 (2021)

105. C. Mauclair et al., Excitation and relaxation dynamics in ultrafast laser irradiated optical glasses. High Power Laser Sci. Eng. **4**, e46 (2016)

106. X. Wang et al., Photochemical response triggered by ultrashort laser Gaussian-Bessel beams in photo-thermo-refractive glass. Optics Express **28**, 31093 (2020)

107. M. Mikutis, T. Kudrius, G. Šlekys, D. Paipulas, S. Juodkazis, High 90% efficiency Bragg gratings formed in fused silica by femtosecond Gauss-Bessel laser beams. Opt. Mater. Exp. **3**, 1862 (2013)

108. Y. Matushiro, W. Watanabe, Femtosecond laser processing of polymethyl methacrylate with an axicon. J. Laser Micro Nanoeng. **11**, 59–65 (2016)

109. W. Watanabe, Y. Matushiro, K. Hatanaka, S. Juodkazis, Regeneration of a grating in PMMA inscribed by femtosecond laser Bessel beam. J. Laser Micro Nanoeng. **12**, 102–106 (2017)

110. K. Homma, W. Watanabe, Fabrication of PDMS-based volume Bragg gratings by stitching of femtosecond laser filament. Jpn. J. Appl. Phys. **60**, 032003 (2021)

111. D. Gailevičius, V. Purlys, K. Staliunas, Photonic crystal spatial filters fabricated by femtosecond pulsed Bessel beam. Optics Letters **44**, 4969 (2019)

112. Q. Sun, T. Lee, M. Beresna, G. Brambilla, Control of laser induced cumulative stress for efficient processing of fused silica. Scientific Reports **10**, 3819 (2020)

113. Z. Wang et al., High-throughput microchannel fabrication in fused silica by temporally shaped femtosecond laser Bessel-beam-assisted chemical etching. Optics Letters **43**, 98 (2017)

114. D. Chu, P. Yao, X. Sun, K. Yin, C. Huang, Ablation enhancement of fused silica glass by femtosecond laser double-pulse Bessel beam. J. Opt. Soc. Am. B **37**, 3535 (2020)

115. A. Rudenko, J.P. Colombier, T.E. Itina, Influence of polarization state on ultrafast laser-induced bulk nanostructuring. J. Laser Micro Nanoeng. **11**, 304–311 (2016)
116. G. Cheng et al., Embedded nanogratings in bulk fused silica under non-diffractive Bessel ultrafast laser irradiation. Appl. Phys. Lett. **110**, 261901 (2017)
117. T. Tamaki, W. Watanabe, J. Nishii, K. Itoh, Welding of transparent materials using femtosecond laser pulses. Jpn. J. Appl. Phys. **44**, L687–L689 (2005)
118. W. Watanabe, S. Onda, T. Tamaki, K. Itoh, J. Nishii, Space-selective laser joining of dissimilar transparent materials using femtosecond laser pulses. Appl. Phys. Lett. **89**, 021106 (2006)
119. S. Richter, F. Zimmermann, R. Eberhardt, A. Tünnermann, S. Nolte, Toward laser welding of glasses without optical contacting. Appl. Phys. A **121**, 1–9 (2015)
120. G. Zhang, R. Stoian, W. Zhao, G. Cheng, Femtosecond laser Bessel beam welding of transparent to non-transparent materials with large focal-position tolerant zone. Optics Express **26**, 917 (2018)
121. S. Hecker, M. Blothe, T. Graf, Reproducible process regimes during glass welding by bursts of subpicosecond laser pulses. Applied Optics **59**, 11382 (2020)
122. G. Martin et al., Near infrared spectro-interferometer using femtosecond laser written gls embedded waveguides and nano-scatterers. Optics Express **25**, 8386 (2017)
123. C. D'Amico, G. Martin, J. Troles, G. Cheng, R. Stoian, Multiscale laser written photonic structures in bulk chalcogenide glasses for infrared light transport and extraction. Photonics **8**, 211 (2021)
124. G. Zhang, G. Cheng, M. Bhuyan, C. D'Amico, R. Stoian, Efficient point-by-point Bragg gratings fabricated in embedded laser-written silica waveguides using ultrafast Bessel beams. Optics Letters **43**, 2161 (2018)
125. K.M. Aghdami, A. Rahnama, E. Ertorer, P.R. Herman, Laser nano-filament explosion for enabling open-grating sensing in optical fibre. Nature Communications **12**, 6344 (2021)
126. X. Liu et al., Front-surface fabrication of moderate aspect ratio micro-channels in fused silica by single picosecond Gaussian–Bessel laser pulse. Appl. Phys. A Mater. Sci. Process. **124**, 206 (2018)
127. X. Liu et al., Truncated Gaussian-Bessel beams for short-pulse processing of small-aspect-ratio micro-channels in dielectrics. Optics Express **27**, 6996 (2019)
128. O. Jedrkiewicz, D. Valetti, P.D. Trapani, Etching and drilling of through-holes in thin glass by means of picosecond Bessel beams. SN Appl. Sci. **1**, 1267 (2019)
129. V.V. Belloni, V. Sabonis, P.D. Trapani, O. Jedrkiewicz, Burst mode versus single-pulse machining for Bessel beam micro-drilling of thin glass: study and comparison. SN Appl. Sci. **2**, 1589 (2020)
130. V.V. Belloni, M. Bollani, S.M. Eaton, P.D. Trapani, O. Jedrkiewicz, Micro-hole generation by high-energy pulsed Bessel beams in different transparent materials. Micromachines **12**, 455 (2021)
131. S. Butkus, D. Paipulas, R. Sirutkaitis, E. Gaižauskas, V. Sirutkaitis, Rapid cutting and drilling of transparent materials via femtosecond laser filamentation. J. Laser Micro Nanoeng. **9**, 213–220 (2014)
132. Y. Ito, R. Yoshizaki, N. Miyamoto, N. Sugita, Ultrafast and precision drilling of glass by selective absorption of fiber-laser pulse into femtosecond-laser-induced filament. Appl. Phys. Lett. **113**, 061101 (2018)
133. Y. Ito, R. Shinomoto, A. Otsu, K. Nagato, N. Sugita, Dynamics of pressure waves during femtosecond laser processing of glass. Optics Express **27**, 29158 (2019)
134. M. Kumagai et al., Advanced dicing technology for semiconductor wafer—stealth dicing. IEEE Trans. Semiconduct. Manuf. **20**, 259–265 (2007)
135. K. Mishchik et al., Dash line glass- and sapphire-cutting with high power USP laser, in *Frontiers in Ultrafast Optics: Biomedical, Scientific, and Industrial Applications XVI*, vol. 9740, ed. by A. Heisterkamp, P.R. Herman, M. Meunier, S. Nolte (International Society for Optics and Photonics (SPIE), 2016), pp. 91–106
136. F. Ahmed, M.S. Lee, H. Sekita, T. Sumiyoshi, M. Kamata, Display glass cutting by femtosecond laser induced single shot periodic void array. Appl. Phys. A **93**, 189–192 (2008)

137. W.J. Tsai, C.J. Gu, C.W. Cheng, J.B. Horng, Internal modification for cutting transparent glass using femtosecond Bessel beams. Optical Engineering **53**, 051503 (2013)
138. M.K. Bhuyan et al., High-speed laser-assisted cutting of strong transparent materials using picosecond Bessel beams. Appl. Phys. A Mater. Sci. Process. **120**, 443–446 (2015)
139. C. Ungaro et al., Using phase-corrected Bessel beams to cut glass substrates with a chamfered edge. Applied Optics **60**, 714 (2021)
140. J. Li, E. Ertorer, P.R. Herman, Ultrafast laser burst-train filamentation for non-contact scribing of optical glasses. Optics Express **27**, 25078 (2019)
141. J. Dudutis et al., In-depth comparison of conventional glass cutting technologies with laser-based methods by volumetric scribing using Bessel beam and rear-side machining. Optics Express **28**, 32133 (2020)
142. K. Bergner et al., Scaling ultrashort laser pulse induced glass modifications for cleaving applications. Applied Optics **57**, 5941 (2018)
143. A. Feuer, J.U. Thomas, C. Freitag, R. Weber, T. Graf, Single-pass laser separation of 8 mm thick glass with a millijoule picosecond pulsed Gaussian–Bessel beam. Appl. Phys. A Mater. Sci. Process. **125**, 332 (2019)
144. M. Jenne et al., Multi pulse pump-probe diagnostics for development of advanced transparent materials processing. J. Laser Micro Nanoeng. **13**, 273–279 (2018)
145. M. Jenne et al., Pump-probe microscopy of tailored ultrashort laser pulses for glass separation processes, in *Laser-based Micro- and Nanoprocessing XIII*, vol. 10906, ed. by U. Klotzbach, A. Watanabe, R. Kling (International Society for Optics and Photonics (SPIE), 2019), pp. 219–225
146. T. Liu, H. Wei, J. Wu, J. Lu, Y. Zhang, Modulation of crack formation inside single-crystal sapphire using ultrafast laser Bessel beams. Opt. Laser Technol. **136**, 106778 (2021)
147. R. Meyer et al., Single-shot ultrafast laser processing of high-aspect-ratio nanochannels using elliptical Bessel beams. Optics Letters **42**, 4307 (2017)
148. D. Flamm et al., Generalized non-diffracting beams for ultrafast materials processing. in *Frontiers in Ultrafast Optics: Biomedical, Scientific, and Industrial Applications XX*, vol. 11270, ed. by P.R. Herman, M. Meunier, R. Osellame (International Society for Optics and Photonics (SPIE), 2020), pp. 68–75
149. M. Jenne et al., Facilitated glass separation by asymmetric Bessel-like beams. Optics Express **28**, 6552 (2020)
150. J. Dudutis, R. Stonys, G. Račiukaitis, P. Gečys, Aberration-controlled Bessel beam processing of glass. Optics Express **26**, 3627 (2018)
151. J. Dudutis, R. Stonys, G. Račiukaitis, P. Gečys, Glass dicing with elliptical Bessel beam. Opt. Laser Technol. **111**, 331–337 (2019)
152. R. Meyer, R. Giust, M. Jacquot, J.M. Dudley, F. Courvoisier, Submicron-quality cleaving of glass with elliptical ultrafast Bessel beams. Appl. Phys. Lett. **111**, 231108 (2017)
153. R. Beuton et al., Thermo-elasto-plastic simulations of femtosecond laser-induced multiple-cavity in fused silica. Appl. Phys. A Mater. Sci. Process. **124**, 324 (2018)
154. M. Jenne et al., High-quality tailored-edge cleaving using aberration-corrected Bessel-like beams. Optics Letters **43**, 3164 (2018)
155. D. Flamm et al., Structured light for ultrafast laser micro- and nanoprocessing. Optical Engineering **60**, 025105 (2021)
156. G.A. Siviloglou, D.N. Christodoulides, Accelerating finite energy Airy beams. Optics Letters **32**, 979 (2007)
157. P. Polynkin, M. Kolesik, J.V. Moloney, G.A. Siviloglou, D.N. Christodoulides, Curved plasma channel generation using ultraintense Airy beams. Science **324**, 229–232 (2009-04)
158. M. Clerici et al., Laser-assisted guiding of electric discharges around objects. Science Advances **1**, e1400111 (2015)
159. S. Vo, K. Fuerschbach, K.P. Thompson, M.A. Alonso, J.P. Rolland, Airy beams: a geometric optics perspective. J. Opt. Soc. Am. A **27**, 2574 (2010)
160. E. Greenfield, M. Segev, W. Walasik, O. Raz, Accelerating light beams along arbitrary convex trajectories. Phys. Rev. Lett. **106**, 213902 (2011)

161. L. Froehly et al., Arbitrary accelerating micron-scale caustic beams in two and three dimensions. Optics Express **19**, 16455 (2011)
162. F. Courvoisier et al., Sending femtosecond pulses in circles: highly nonparaxial accelerating beams. Optics Letters **37**, 1736 (2012)
163. A. Mathis et al., Arbitrary nonparaxial accelerating periodic beams and spherical shaping of light. Optics Letters **38**, 2218 (2013)
164. M.A. Alonso, M.A. Bandres, Generation of nonparaxial accelerating fields through mirrors. i: Two dimensions. Optics Express **22**, 7124–7132 (2014)
165. A. Mathis et al., Direct machining of curved trenches in silicon with femtosecond accelerating beams. JEOS:RP **8**, 13019 (2013)
166. D. Sohr, J.U. Thomas, S. Skupin, Shaping convex edges in borosilicate glass by single pass perforation with an Airy beam. Optics Letters **46**, 2529 (2021)
167. D. Flamm et al., Protecting the edge: Ultrafast laser modified c-shaped glass edges. J. Laser Appl. **34**, 012014 (2022)
168. V. Jukna et al., Filamentation with nonlinear Bessel vortices. Optics Express **22**, 25410 (2014)
169. C. Xie et al., Tubular filamentation for laser material processing. Scientific Reports **5**, 8914 (2015)
170. W. Cheng, P. Polynkin, Micromachining of borosilicate glass surfaces using femtosecond higher-order Bessel beams. J. Opt. Soc. Am. B **31**, C48 (2014)
171. O. Jedrkiewicz, S. Bonanomi, M. Selva, P.D. Trapani, Experimental investigation of high aspect ratio tubular microstructuring of glass by means of picosecond Bessel vortices. Appl. Phys. A Mater. Sci. Process. **120**, 385–391 (2015)
172. J., Baltrukonis, O. Ulčinas, S. Orlov, V. Jukna, Void and micro-crack generation in transparent materials with high-energy first-order vector Bessel beam. J. Opt. Soc. Am. B **37**, 2121 (2020)
173. E. Nacius et al., Spatially displaced and superposed Bessel beams for transparent material laser micro-processing. J. Opt. Soc. Am. B (2021)
174. P. Šlevas, S. Orlov, E. Nacius, O. Ulčinas, Azimuthally modulated axicon vortical beams for laser microprocessing. Optics Communications **505**, 127509 (2022)
175. S. Orlov, A. Juršenas, E. Nacius, Optical Bessel-like beams with engineered axial phase and intensity distribution. J. Laser Micro Nanoeng. **13**, 244–248 (2018)
176. X. Yu, C.A. Trallero-Herrero, S. Lei, Materials processing with superposed Bessel beams. Appl. Surf. Sci. **360**, 833–839 (2016)
177. A. Zannotti, C. Denz, M.A. Alonso, M.R. Dennis, Shaping caustics into propagation-invariant light. Nature Communications **11**, Article number: 3597 (2020)
178. T. Dietz et al., Ultrafast thin-disk multi-pass amplifier system providing 19 kW of average output power and pulse energies in the 10 mJ range at 1 ps of pulse duration for glass-cleaving applications. Optics Express **28**, 11415 (2020)
179. A. Vailionis et al., Evidence of superdense aluminium synthesized by ultrafast microexplosion. Nature Communications **2**, Article number: 445 (2011)